

Robustness improvements for 2D reinforced concrete moment resisting frames: Parametric study by means of NLFE analyses

*Original*

Robustness improvements for 2D reinforced concrete moment resisting frames: Parametric study by means of NLFE analyses / Miceli, E.; Castaldo, P.. - In: STRUCTURAL CONCRETE. - ISSN 1464-4177. - ELETTRONICO. - 25:1(2024), pp. 9-31. [10.1002/suco.202300443]

*Availability:*

This version is available at: 11583/2985807 since: 2024-02-08T16:11:10Z

*Publisher:*

John Wiley and Sons

*Published*

DOI:10.1002/suco.202300443

*Terms of use:*


This article is made available under terms and conditions as specified in the corresponding bibliographic description in the repository

*Publisher copyright*

(Article begins on next page)

## ARTICLE

# Robustness improvements for 2D reinforced concrete moment resisting frames: Parametric study by means of NLFE analyses

Elena Miceli  | Paolo Castaldo 

Department of Structural, Geotechnical and Building Engineering (DISEG), Politecnico di Torino, Turin, Italy

## Correspondence

Elena Miceli, Department of Structural, Geotechnical and Building Engineering (DISEG), Politecnico di Torino, Turin, Italy.  
Email: [elena.miceli@polito.it](mailto:elena.miceli@polito.it)

## Funding information

European Union Next-GenerationEU

## Abstract

This study develops a 2D computational parametric analysis of ordinary reinforced concrete (RC) frames, located in seismic zone, with the aim to evaluate some design suggestions with respect to their effectiveness in increasing the structural robustness. Specifically, a five-storey and four-span 2D RC moment resisting frame is considered, designed in a highly seismic area according to both Italian and European codes. Subsequently, respecting the seismic design code provisions through a cyclic design procedure, some modifications are suggested regarding the layout of the longitudinal reinforcement bars of the beams to exploit the continuity, Vierendeel behavior and influence of the side face reinforcement bars in the beams. For the different modifications, nonlinear finite element pushdown analyses of the whole frames are performed by imposing a monotonically increasing vertical displacement at the point of the column removal in Atena-2D and considering the presence of the orthogonal framed systems. Furthermore, two different failure scenarios are examined. The numerical force-displacement capacity curves corresponding to the different proposed design suggestions are investigated and compared. The results have demonstrated the effectiveness in improving the structural robustness of the proposed solutions, especially, of the side face reinforcement bars with respect to both flexural and catenary behavior. The outcomes have also highlighted the compatibility between design criteria of both robustness and earthquake engineering.

## KEYWORDS

cyclic design process, NLFE capacity curve, RC MR frame, side face reinforcement bars, structural robustness, Vierendeel behavior

## 1 | INTRODUCTION

The topic of structural robustness is becoming increasingly relevant within structural engineering due

to the occurrence of catastrophic events such as, for instance, the gas explosion in the Ronan Point Tower (London, May 16, 1968), the Alfred P. Murrah Federal Building terrorist attacks (Oklahoma, April 19, 1995), the

This is an open access article under the terms of the [Creative Commons Attribution-NonCommercial-NoDerivs](https://creativecommons.org/licenses/by-nc-nd/4.0/) License, which permits use and distribution in any medium, provided the original work is properly cited, the use is non-commercial and no modifications or adaptations are made.

© 2023 The Authors. *Structural Concrete* published by John Wiley & Sons Ltd on behalf of International Federation for Structural Concrete.

World Trade Center attacks (New York, September 11, 2001). Those events caused dramatic consequences in terms of lives lost together with social, economic, and environmental impacts. Regarding the definition of robustness<sup>1</sup> within structural and earthquake engineering,<sup>2,3</sup> structures that, in the event of a local damage, are not susceptible to a damage spread or a collapse, are defined robust; therefore, robustness indicates the level of insensitivity of a structure to a local damage. Moreover, “Eurocode—Basis of structural design”<sup>4</sup> indicates that a structure must be designed and built in such a way that it should not be damaged by events such as fire, explosions, impacts or the consequences of human errors to an extent disproportionate to the original cause.

In this context, it is important to outline the scientific activities aimed at defining the levels of risk and developing prescriptive tools as well as guidelines and provisions over the world (e.g., Refs. 5–12) to support the designers in the decisional phases, both for new and existing structural systems. Specifically, most of these standards recognize the need of adopting continuity between structural elements and, in particular, continuation of longitudinal reinforcement through supports, as well as symmetric longitudinal reinforcement in the beams across a column.

Previous studies have investigated the influence of some parameters in order to enhance a robust design in case of reinforced concrete (RC) buildings: the importance of increasing the longitudinal reinforcement to improve the load bearing capacity and, at the same time, the need of reducing the stirrup step to reduce flexural-shear interaction causing brittle failure<sup>13</sup>; the benefits of arranging the longitudinal reinforcement in a symmetric manner in order to increase the bending capacity of beams when the removal of a column causes a switch in the moment sign.<sup>14</sup> The positive effects of different structural parameters (i.e., slab thickness and seismic reinforcement) on the progressive collapse resistance of beam-slab substructures through experimental tests are examined in Refs. 15,16 These works also concluded that an increase in the height of the beam is beneficial but only for the beam behavior and does not influence the catenary behavior. A full-scale building was tested in Adam et al.,<sup>17</sup> analyzing the capability of the structure to exploit flexural and Vierendeel beam actions as alternative load paths in case of corner column removal. The parametric analysis on RC frames under corner column loss of Zhang et al.<sup>18</sup> demonstrated that the collapse-resistance capacity increases with the height of the beam section and the percentage of the lower steel reinforcing bars of the beam. However, larger heights of the beams are associated to weaker rotation capacity of beam-column joints and ductility of the frame.

The beneficial effects of RC slab strips thanks to the development of catenary actions have been discussed in Belletti et al.<sup>19</sup> In Tan et al.,<sup>20</sup> experimental works on multi-storey planar steel sub-frames are described and numerically simulated, in order to study the effects of different boundary constraints on the collapse behavior, including the positive effects of a RC slab. Moreover, an experimental and numerical study on a beam-column RC sub-structure is described in Wang et al.,<sup>21</sup> to evaluate the effects of transverse beams and the slab. Similarly, the research developed in Fascetti et al.<sup>22</sup> has highlighted the advantages when the effects of transverse elements are considered, leading to the importance of including the three-dimensionality in the plane model. This conclusion was also reached in Brunesi and Parisi<sup>23</sup> by comparing the results of 2D and 3D models in terms of incremental dynamic analyses, demonstrating how secondary beams represent a source of additional stiffness and resistance in case of base-column loss scenario. The strength and stiffness increase against vertical collapse in infilled frames with respect to bare frames is demonstrated in Di Trapani et al.,<sup>24</sup> also studying the influence of many geometric and mechanical parameters.

Other works are mainly focused on theoretically quantifying structural robustness. In Asprone et al.,<sup>25</sup> a robustness matrix based on a measure of the accidental events types and intensities is defined. In Izzuddin and Sio,<sup>26</sup> a simplified tying force method is elaborated to evaluate progressive collapse performance of different RC systems. An analytical model is studied to evaluate the ultimate bearing capacity of one-way and two-way RC slabs<sup>27</sup> and RC flat slabs<sup>28</sup> in case of column loss scenarios. A piecewise multi-linear curve is numerically obtained in Pham and Tan,<sup>29</sup> to predict the structural response of RC beam-column sub-assemblages under column loss events.

Some advantages of seismic detailing for RC structures are commented in Refs. 30–32 For instance, the results in Refs. 33,34 underlined that if the Alfred P. Murrah Federal Building had been designed with seismic detailing, a reduction of damage of 50% could have occurred. On the other hand, although seismic design can increase the load-bearing capacity of the members, it is not always enough to guarantee resistance against progressive collapse.<sup>13</sup>

Most the abovementioned literature studies have evaluated the robustness of RC structures by means of sub-assemblies or carrying out theoretical or 3D fiber-based analyses with specific assumptions.

This study aims to increase the robustness of a 3D RC building in seismic zone by improving the design of the plane frames. In this way, it presents a 2D computational parametric analysis of ordinary RC moment resisting

(MR) frames, designed in a highly seismic area, with the aim to evaluate some design suggestions with respect to their effectiveness in increasing the structural robustness. Specifically, a five-storey and four-span 2D RC MR frame is considered, designed in a highly seismic area according to both Italian<sup>35</sup> and European<sup>36</sup> codes. Subsequently, some modifications are suggested, always respecting the seismic design code provisions by means of a cyclic design procedure. In detail, different configurations of longitudinal reinforcement bars of the beams have been proposed with respect to the continuity and Vierendeel behavior as well as the benefits of accounting for side face reinforcement bars in the beams are deepened. Furthermore, two different failure scenarios are investigated. For the different improvements, 2D nonlinear finite element (NLFE) pushdown analyses of the whole frames are performed by imposing a monotonically increasing vertical displacement at the point of the column removal and considering the influence of the orthogonal framed structures. The numerical force-displacement capacity curves corresponding to the different proposed design suggestions are investigated and compared. Regarding both failure scenarios, the results have demonstrated the effectiveness in improving the structural robustness of the proposed solutions, such as the arrangement of the longitudinal rebars, presence of the side face rebars and adoption of the same amount of longitudinal reinforcement in some or all floors in order to exploit the Vierendeel effects. These improvements turned out to be effective with respect to both flexural and catenary behavior. The outcomes have also showed the compatibility between robustness and earthquake engineering design criteria for RC MR frames.

## 2 | ROBUSTNESS OF A 2D RC FRAME: THE PUSHDOWN OR CAPACITY CURVE

RC members present a nonlinear response, especially, after formation of concrete cracks and yielding of reinforcing bars. Moreover, in presence of large displacements, consequential to the removal of a column, the so-called geometrical nonlinearity outcomes take place, which must be considered. Therefore, nonlinear static analyses permit to investigate the structural response, even if the dynamic effects are not accounted for Refs.<sup>37,38</sup> In this way, the displacement-controlled pushdown analysis is effective to define the resulting capacity curves.<sup>39–41</sup> The nonlinear analysis can be carried out by defining a NL numerical model and imposing a monotonically increasing vertical displacement to the point at the top of the removed column, obtaining, as a result of each step,

the force that the rest of the structure is able to provide at the same point. The resulting curve is the so-called force-displacement capacity curve or reaction-displacement capacity curve or pushdown curve.<sup>39–41</sup>

The structural behavior of RC MR frames subjected to this failure scenario can be characterized by three phases: (i) the first phase (i.e., *flexural behavior*) depends on the bending behavior of the beam and lasts with the formation of plastic hinges at the connection points between beam and column. The lateral points are displaced toward the external part, because of the cracking and consequent elongation of the beam (i.e., outward horizontal displacements). In fact, the beam is subjected to compressive arching forces because of the stiffness of the columns that oppose the beam elongation; (ii) the second phase (i.e., *softening*) is characterized by a softening response with a reduction of the reaction at the point where the column is removed. The compressive arching forces and, consequently, the horizontal displacements start to reduce; (iii) the third phase (i.e., *catenary effect*) presents an increase of the reaction for increasing vertical displacement in the point of removal. The horizontal displacements reduce and change sign (i.e., the external columns move toward the inner part), being the beam in tension. This derives from a combination of the flexural and catenary effects in the rebars.

It is important to underline that if the reinforcement does not continue over the external columns, the softening is not possible and only flexural behavior of the beam takes the load.<sup>12</sup>

Within the capacity curve, the maximum resistant load in the flexural phase (i.e., flexural peak) is denoted as  $P_{MAX,FL}$ , whereas the maximum resistant load at the end of the curve (i.e., ultimate resistance) is identified as  $P_{MAX,RES}$ . Various experimental results<sup>15,16,21,42–45</sup> highlighted that the activation of catenary effect coincides with a displacement equal to almost the depth of the beam.

Following the energetic approach by Izzuddin et al.,<sup>41</sup> the capacity curve with these peak resistances defines the internal work, whereas the external work is provided by the external action. This latter can be assumed equal to the corresponding reaction  $P_{EXT}$  of the column<sup>8,11</sup> before the removal and depends on the loads (i.e., permanent structural loads, non-structural loads, and variable loads) within the accidental combination according to the codes.<sup>35,36</sup> In addition, this external reaction  $P_{EXT}$ , because of the dynamic effects caused by the removal of the column, must be increased by a dynamic coefficient  $\lambda$  obtaining  $P_{EXT,DYN}$ . If the capacity curve accounts for the self weight, the external reaction  $P_{EXT,DYN}$  should consider only the dynamically amplified rate of the self weight, as follows:

$$P_{EXT,DYN} = \lambda P_{EXT} + (\lambda - 1)P_{SW} \quad (1)$$

where  $P_{SW}$  is the external reaction due to the self weight, that has not to be considered in  $P_{EXT}$ . When NL simulations are carried out, the dynamic coefficient  $\lambda$  assumes values in the range 1–1.5.<sup>17,46</sup> Indeed, the energetic approach<sup>41</sup> represents a very useful methodology for the assessment of  $\lambda$  given the knowledge of the capacity curve and to identify the performance point on the capacity curve (i.e., when the internal energy equals the external work). Therefore, the evaluation of the capacity curve is fundamental for a robustness-based design.

### 3 | DESIGN SUGGESTIONS TO IMPROVE THE ROBUSTNESS

With the aim to improve the robustness of a RC structural system, different literature studies together with codes provide important provisions as follows:

- **Support-continuity:** according to design load scenarios related to ultimate limit state (ULSs) and service limit states (SLSs) and seismic verifications, the beams are designed with a non-constant longitudinal reinforcement, but larger in the most stressed sections. As for a sudden loss of a supporting column, the beams have to assume a tie behavior and this is possible through continuous longitudinal reinforcement bars over the supports<sup>5–7,12,17</sup>;
- **Section symmetry (S):** referring to design load scenarios related to ULSs, SLSs, and seismic verifications, the value and sign of the bending moment in the spans of the beams are different from the ones of the moment at the supports, so the bottom longitudinal reinforcement is different from the top one. When loss of a load-bearing column occurs, some sections undergo to opposite bending moments. Therefore, the second suggestion<sup>5,14</sup> consists in providing the same reinforcement in the two chords of the beam, making the section symmetrical;
- **Lateral springs:** the presence of the orthogonal structural systems can highly and positively influence the response of the structure when a supporting column collapses, as demonstrated in Refs.<sup>19–21,47–51</sup> In general, the horizontal flexural-shear response of the orthogonal beams combined with the slabs can produce “3D effects” with important benefits.

In this study, the continuity as well as the elastic springs, related to the contribution of the orthogonal systems, are considered, as explained in the next sections. Inspired by Refs.,<sup>12,17</sup> the following robustness

suggestions are proposed in addition or substitution of the section symmetry (S) recommendation:

- **Continuity (C):** the continuity is intended as having all the longitudinal reinforcement bars continuous over the supports and increasing the length of the longitudinal rebars in the upper chord of the beams, at each edge of the beams, until 1.5 m from the column axis (i.e., 30% of the span length) in addition to the anchorage length. This derives from the major extension of the bending moment in the upper chord of the beams due to the column loss. This is finalized to avoid plastic hinges in cross-sections with lower flexural resistance and ductility;
- **Global floor equality (E):** the longitudinal reinforcement in the beams of the lower floors is typically higher, because of higher external bending moments within the seismic combination. In the case of a supporting column loss, due to the reduced axial extensibility of the column, all floors can be assumed subjected to the same displacement in correspondence of the removed column and, therefore, to the same internal actions (i.e., Vierendeel behavior). Thus, it is suggested to apply to all the floors the same amount of reinforcement of the first floor (i.e., the largest one).
- **Partial floor equality (PE):** this suggestion has the same reasons of the previous one (i.e., to take advantage of the Vierendeel effects) but consists in applying only to the last floor the same amount of longitudinal reinforcement of the first one;
- **Side face rebars:** the presence of the side face reinforcement bars can play a crucial role to anticipate the transition toward the catenary activation at lower vertical displacements. In fact, since they are located close to the section geometric barycenter, their contribution to flexural response is reduced and so can provide an important contribution to a tension response facilitating tie behavior. The proposal is to include these rebars in the design and numerical analyses.

Obviously, by applying all or some of the proposed modifications to the longitudinal reinforcement arrangement of the beams, the resistant moments in the sections change, and this influences the seismic design with respect to the capacity design principles. A cyclic redesign is, thus, proposed to achieve a compatibility between robustness and seismic design as shown in Figure 1 and discussed later.

In the following, the above-mentioned robustness improvements together with the cyclic redesign are numerically tested for a RC MR frame in seismic zone by combing all or some of the proposed suggestions in order to investigate both the flexural behavior and catenary

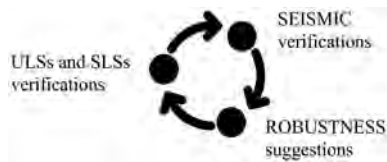


FIGURE 1 Representation of the cyclic design process.

effects for two failure scenarios as well as to optimize the amount of reinforcement layout. It is worth underling that the presence of the catenary stage in the capacity curves can ensure a stable structural performance in case of a progressive collapse with large dynamic effects.

## 4 | DESIGN OF 2D RC MR FRAMES IN SEISMIC ZONE

To assess the effectiveness of the suggestions, the starting point is the design of a 2D multi-storey RC MR frame, consisting of four floors plus roof, four spans, regular in elevation and symmetrical. The design is carried out following the seismic design guidelines of both NTC2018<sup>35</sup> and EC8,<sup>36</sup> assuming L'Aquila city (Italy) as reference site and a high ductility class. The frame has spans with length of 5 m, inter-storey height of 3 m and transverse influence width of 5 m (Figure 2). All the beams have dimensions of 40 × 50 cm, while columns have 60 × 60 cm sections. A large height of the beam has been selected in line with the need of achieving a larger bearing capacity in flexural stage.<sup>15–17</sup> This can be beneficial to reach earlier the performance point in terms of energetic equivalence.<sup>41</sup> At the same time, a relatively large height-to-width ratio of the beam (i.e., 80%) derives from the need of facilitating a more ductile behavior in the post-peak stage to reach the activation of the catenary.<sup>24</sup> The RC slabs present joists along one direction (Figure 2a), typical in some countries (e.g., Italy).

Regarding the reinforcement, B450C steel reinforcing bars<sup>35</sup> are used:  $\phi 18$  for the longitudinal reinforcement of the beams,  $\phi 20$  for the columns and  $\phi 8$  for the stirrups of both the structural elements. In addition, C25/30 concrete<sup>35</sup> with 3.5 cm of concrete clear cover is used in any element.

All the different gravity loads combined with the snow and wind actions according to NTC2018<sup>35</sup> and EC8<sup>36</sup> are considered. Moreover, the seismic actions derived from the different combinations<sup>35,36</sup> have been considered within the numerical code SAP2000.<sup>52</sup> Regarding ULSs and SLSs verifications and the capacity-design principles for the different seismic code LSs, the structural detailing is computed. Figure 3a illustrates the reinforcement detailing obtained from the

verifications. The transversal reinforcement in the beams is made of 2-legs  $\phi 8$  stirrups arranged with a spacing of 10 cm in the dissipative zone and 15 cm in the central zones of the spans, for all the floors.

As for the columns reinforcement (Figure 3b), the use of 12 $\phi 20$  longitudinal reinforcing bars is obtained for the bending reinforcement (located symmetrically in both directions), while the shear reinforcement consists of 4-legs  $\phi 8$  with a spacing of 10 cm, along the entire length of the structural element apart from the nodes (i.e., beam-column nodes) where the spacing is equal to 5 cm.

## 5 | DEFINITION OF NLFE MODEL TO SIMULATE THE FAILURE SCENARIOS

This section deals with the definition of the 2D NLFE models of the 2D RC frame (i.e., Figure 2) finalized to investigate the capacity curves with the possible catenary effects, assuming the removal of a base column as the local failure scenario induced, for example, by detonation or explosion or foundation failure. In this study, two different failure scenarios are considered: first, the removal of the central column, then, the removal of the second to last column (Figures 5 and 6). Only these two failure scenarios together with the specific frame under study are examined since they represent the worst situations in a 3D building where any contribution deriving from infills<sup>19,22,24</sup> is absent. Only by means of 2D FE simulations, it is possible to consider the nonlinear response of the RC frame with respect to ductile or brittle failures in local or global resistance mechanisms for the proposed robustness suggestions characterized by different modifications in the floors. 3D FEM analyses are not necessary since the study aims to increase the robustness of a 3D RC building in seismic zone by improving the design of the plane frames. This is a safe design scope for buildings, especially, with RC slabs having joists along one direction.

To carry out these analyses, the FE software Atena-2D<sup>53</sup> is used. Four-node quadrilateral iso-parametric plane stress finite elements are adopted, with an element thickness in the transverse direction of 60 cm for the columns and 40 cm for the beams and selecting the *Element size*, that is, the mesh size, varying between 0.05 and 0.1 m. The choice of the element size derives from an iterative process of numerical accuracy. The equations are solved by means of standard Newton–Raphson iterative procedure based on a linear approximation hypothesis. The tolerances are set equal to 1.0% for the norm of displacement error, varying from 1.0% to 1.5% for both

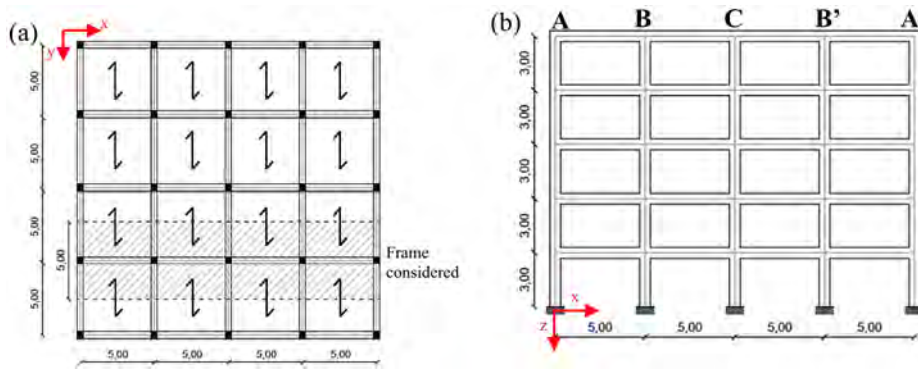


FIGURE 2 Geometry of the multi-storey reinforced concrete moment resisting frame: (a) plan view with joists framework direction; (b) lateral view. Measurements in m.

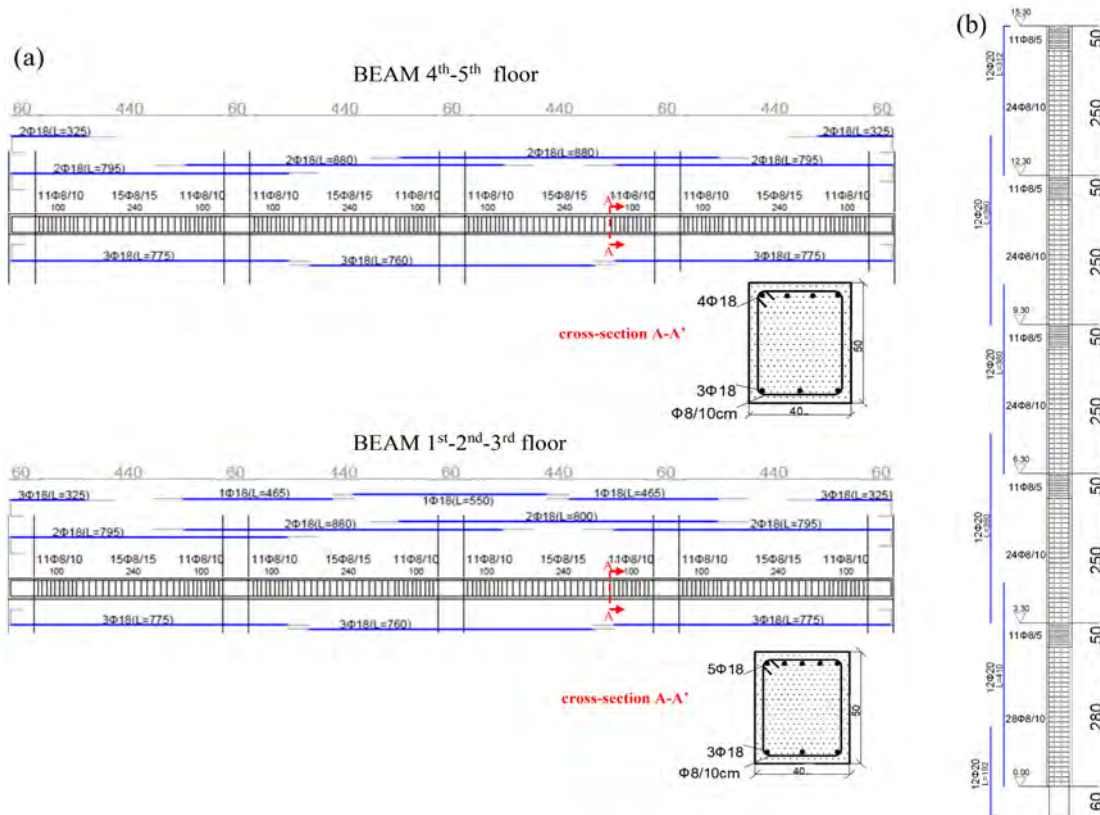


FIGURE 3 Longitudinal and transverse reinforcement arrangement for: (a) beams with the cross-sections; (b) columns. Measurements in cm. Indication of position of two cross sections in the beams.

the norm of residual force error and maximum error of residual forces and 1.0‰ for the out-of-balance energy error (as suggested in Refs.<sup>54,55</sup>). The maximum number of iterations for each step is set equal to 2500.

Two materials (i.e., concrete and reinforcing steel) are modeled as follows to consider the mechanical nonlinearities in addition to the geometrical ones.

As for the first material (i.e., C25/30<sup>35</sup>), concrete is modeled as *SBeta Material*, for which the formulation of constitutive models is considered in the plane stress state. Regarding the tensile behavior, a “local strain” tension softening type model is considered, where the

tension stiffening effect<sup>54</sup> is included by means of a linear post-peak branch up to the zero strength in correspondence of a strain equal to  $10f_{ctm}/E_{cm}$ , being  $f_{ctm}$  the mean value of the tensile strength (i.e., 2.56 MPa) and  $E_{cm}$  the mean secant elastic modulus, computed according to Starossek.<sup>2</sup> Furthermore, the cracking process has been reproduced using the “Smearred cracking” with fixed crack direction model.<sup>56,57</sup> With reference to the behavior in compression, the nonlinear response is introduced by selecting the “Softening Modulus” option. In detail, the compression before the peak stress is derived by the formula recommended in CEB-FIP Model Code 90,<sup>58</sup> while

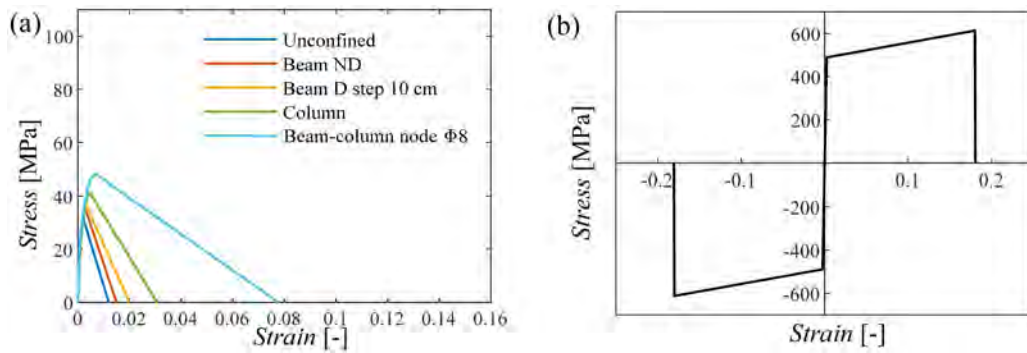


FIGURE 4 Constitutive laws: (a) concrete compressive behavior; (b) steel tensile and compressive behavior.

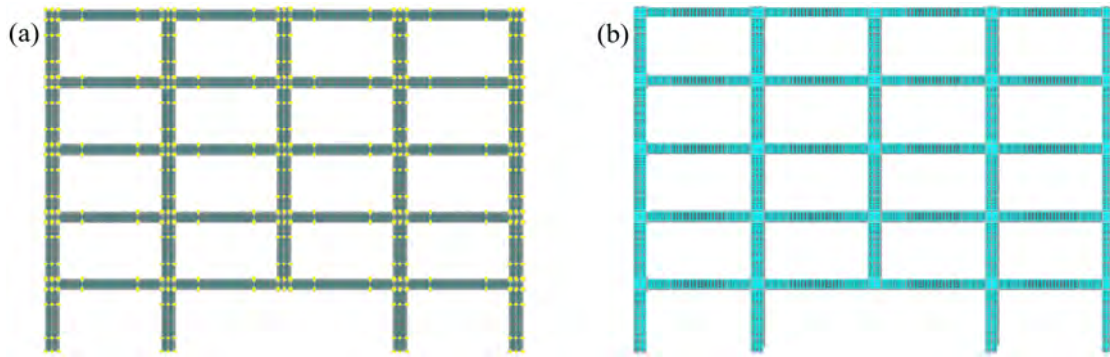


FIGURE 5 Representation of the 2D nonlinear finite element model for the first failure scenario with: (a) joints, lines, macro-elements, and mesh; (b) longitudinal and transversal reinforcement.

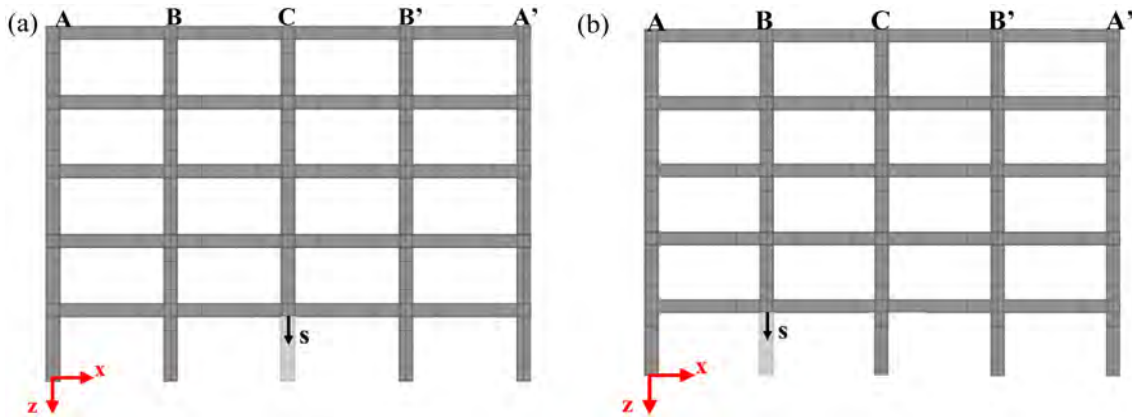


FIGURE 6 Nonlinear finite element pushdown analysis schemes for the (a) first and (b) second failure scenarios.

the post-peak compression is linearly descending and it is based on a local strain softening according to Saatcioglu and Razvi model,<sup>59</sup> which accounts for the multiaxial state of stress. Specifically, the post-peak elastic modulus  $E_d$  is the slope of the post-peak branch in correspondence to a reduction of stress after the peak equal to 15%. The parameter to consider the reduction of compressive strength due to cracks is set equal to 0.8, which represents the maximal strength reduction under the large

transverse strain, in line with the experimental results of Dyngeland.<sup>60</sup> The compressive behavior of concrete is shown in Figure 4a. Specifically, the constitutive model in compression has been derived for: unconfined concrete (i.e., concrete effective cover—“unconfined”), concrete in non-dissipative areas of beams (“beam ND”), concrete in dissipative area of beams (“beam D” considering the step of the stirrups), concrete in columns, concrete in beam-column nodes (considering the stirrup



diameter). Finally, a variable shear retention factor<sup>61</sup> is assumed to consider the reduction of shear stiffness due to cracks occurrence.

Regarding the second material, B450C reinforcing steel<sup>35</sup> is defined by the *Reinforcement* material type. A bi-linear curve with hardening constitutive law both in tension and in compression is considered assuming the mean values of the mechanical properties as shown in Figure 4b. Moreover, both steel longitudinal and transverse reinforcement are modeled as “discrete bar” elements (i.e., truss elements), assuming a perfect bond with the concrete. The yielding strength is equal to the mean value of B450C reinforcing steel (i.e., 489 MPa), while the ultimate strength is equal to 611 MPa (i.e., by considering an ultimate-to-yielding strength ratio equal to 1.25 as suggested by Ref.<sup>35</sup>). The ultimate strain is assumed equal to 0.18. This last assumption, together with the ultimate-to-yielding ratio, are in accordance with different experimental tests investigating the robustness of RC sub-assemblies<sup>15,16,43–45,47,52–63</sup> as well as in line with the results of monotonic tensile tests conducted on a wide range of steel reinforcing specimens.<sup>64</sup> The elastic modulus is equal to 210 GPa.<sup>2</sup>

The geometrical characteristics of the frame are included by modeling the points, lines, and macro-elements (i.e., quadrilateral elements) as shown in Figure 5 for the first failure scenario. As it can be observed, the frame is modeled without the related base column and the step-by-step evolution of the structural behavior is studied by applying a vertically imposed displacement at the top point of the removed column, without considering any other action apart from the self-weight. In this way, it is possible to perform displacement-controlled NLFE push-down analyses and assess the structural response as well as the deformation, crack pattern and stress state, investigating the residual resistance of the structure (i.e., capacity curve). Furthermore, steps of 1 cm imposed displacement have been considered. Finally, fully fixed constraints are considered at the bottom of each column.

Note that a vertical or horizontal displacement is positive if it respects the orientation of the axis  $z$  or  $x$ , respectively, as illustrated in Figure 6 for the two failure scenarios.

## 6 | THE FIRST FAILURE SCENARIO: NLFE ANALYSES OF THE RC MR FRAME FOR THE DIFFERENT ROBUSTNESS IMPROVEMENTS

This section presents the capacity curves achieved from several NLFE simulations of the RC MR frame corresponding to the different design suggestions to increase the robustness capability of the structural system. Table 1 summarizes all the analyses conducted for various

combinations of the different improvements together with the corresponding nomenclatures or acronyms. The failure scenario corresponding to the central column removal (i.e., column C) is commented in this section.

### 6.1 | STANDARD model

In Figure 7a, the NLFE pushdown curve is shown for the frame designed according to the current code rules, denoted as “*STANDARD*.” The design respects only the continuity over the supports. The value of  $P_{MAX,FL}$  is equal to 811 kN; after the flexural peak, the model shows a softening phase followed by a failure in correspondence of  $P_{MAX,RES}$  equal to 738 kN. This drop is reached at an imposed displacement of around 20 cm due to the formation of concentrated curvatures in critical areas. These critical areas (Figure 7b) are located in the beams where there is the transition from dissipative to non-dissipative zone with changes in both the longitudinal and transverse reinforcement arrangement.

It is noteworthy that the shear capacities of the beams close to the column removed are equal to 158.6 and 264.4 kN, respectively, in the dissipative and non-dissipative area, and are not overcome.

The structure does not show any catenary behavior. In fact, there is an increasing outward horizontal movement of the columns (Figure 7c), due to the arching behavior of the beams, without any shift in sign. At the same time, Figure 7d shows that the column B, which is the closest to the collapsed area, tends to first move downward due to the flexural behavior and then, because of the arching behavior of the beams, tend to move upward following the rotation of the nodes. On the other hand, being external, the nodes of the column A are less influenced by the initial flexural stage.

### 6.2 | Models with continuity, symmetry, and springs

This subsection deals with three modifications: continuity, symmetry, and orthogonal contribution.

The modification of reinforcement bars in the frame is initially evaluated applying the continuity criterion. In particular, continuous longitudinal rebars are arranged along each beam as proposed in Section 3: this model is identified with the acronym “*C*.” The new arrangement of the longitudinal reinforcement along 1.5 m at two edges of the spans is made of  $3\phi 18$  in the lower chord of all the beams of the five floors, while  $5\phi 18$  in the upper chord for the first three floors and  $4\phi 18$  in the last two floors. Both the ULS and seismic verifications are verified for the new

TABLE 1 Summary of the different types of NLFE analyses.

Model	Support-continuity	Continuity	Section symmetry	Orthogonal contribution	Global floor equality	Partial floor equality	Side face rebars
STANDARD	✓	×	×	×	×	×	×
C	✓	✓	×	×	×	×	×
CS	✓	✓	✓	×	×	×	×
CS + springs	✓	✓	✓	✓	×	×	×
CSE + springs	✓	✓	✓	✓	✓	✓	×
CPE + springs	✓	✓	×	✓	×	✓	×
CSE + springs + rebars	✓	✓	✓	✓	✓	✓	✓
C + springs + rebars	✓	✓	×	✓	×	×	✓
CPE + springs + rebars	✓	✓	×	✓	×	✓	✓

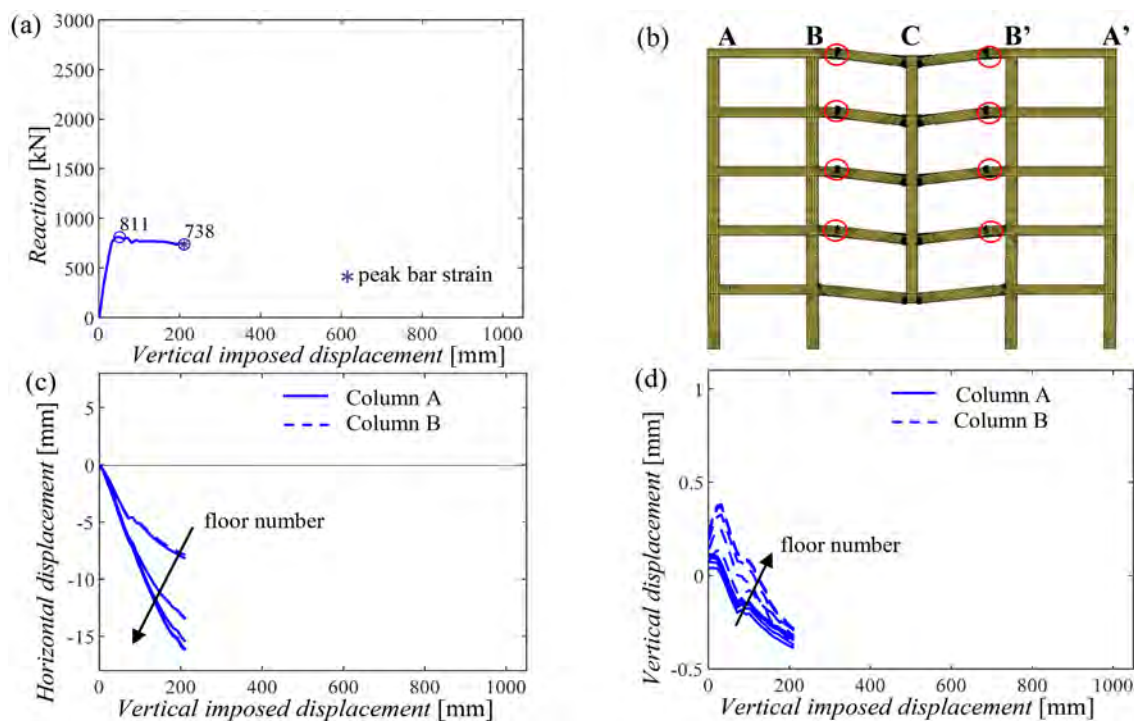


FIGURE 7 Results of the pushdown analysis for the *STANDARD* model: (a) capacity curve; (b) failure mode with the critical regions; (c) horizontal displacements of the beam-column nodes; (d) vertical displacements of the beam-column nodes.

arrangement of the longitudinal reinforcement. Thus, shear reinforcement of the beams, longitudinal, and shear reinforcement of the columns and beam-column nodes remained unchanged (Figures 3 and 4).

The second additional modification is the symmetry in the cross-sections, with the aim to have the same quantity of reinforcing bars between the upper and lower chord, maintaining the continuity. This model, defined

with the acronym “CS,” is characterized by a reinforcing bar arrangement along 1.5 m at two edges of the beams as follows: 5 $\phi$ 18 in both levels for the first three floors (Figure 8b) and 4 $\phi$ 18 above and below in the two remaining floors (Figure 8b). According to the proposed cyclic design process, this modification caused a change of the stirrup steps from 10 to 7.5 cm in the dissipative zone for the beams of the first three floors to respect the seismic

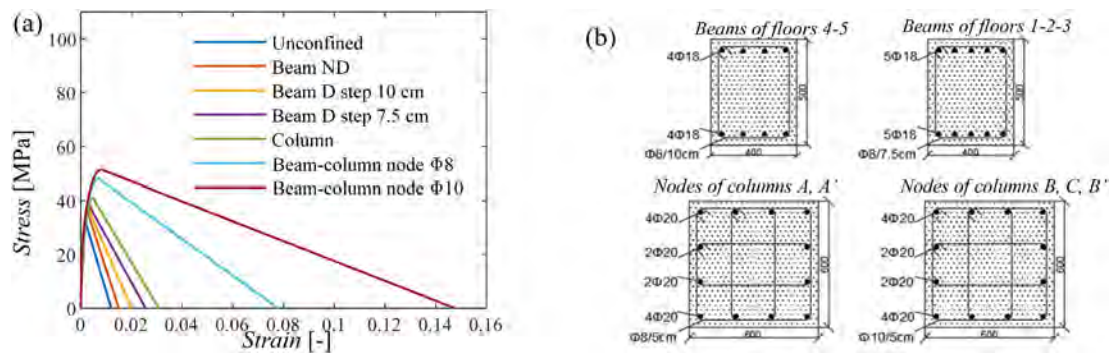


FIGURE 8 CS model: (a) Constitutive laws of concrete in compression; (b) distribution of the longitudinal and transverse reinforcement in the cross-sections of Figure 3a and in the beam-column nodes.

verifications. Similarly, for the beam-column nodes of the columns B, C, and B', a change in the stirrup diameter from  $\phi 8$  to  $\phi 10$  was necessary, maintaining the step of 5 cm. On the other hand, the longitudinal and transverse reinforcement of the columns remained unchanged. Of course, these changes in the transverse reinforcement of beams and nodes also imply a modification of the constitutive law for the confined concrete of the dissipative area for both beams (“beam D step 7.5 cm”) and beam-column nodes (“beam-column node  $\phi 10$ ”) according to Saatcioglu and Razvi.<sup>59</sup> The modifications in terms of constitutive law for concrete in compression together with longitudinal and transverse reinforcement arrangement are illustrated in Figure 8.

Thirdly, the contribution provided by the orthogonal systems to the frame with continuity and symmetry has been modeled by means of elastic springs. In fact, in a 3D building, the lateral displacements of a plane frame are limited due to the influence of the transverse structural elements, which stiffen the structure and surely enhance the robustness.<sup>19,20,24,48–51</sup> However, it is not straightforward to experimentally calibrate the stiffness of the lateral constraints.<sup>29</sup> The lateral constraint conditions, determined by the transverse beams belonging to the orthogonal framed systems and slabs with one-way joists, have been herein modeled, in a simplified way, by means of elastic translational springs. In this work, the rotational stiffness has been discarded since it does not influence the development of catenary action, and has a negligible influence on the flexural peak, as highlighted in Refs.<sup>20,29</sup> The stiffnesses of these translational elastic springs are properly calibrated for each node of the five floors through elastic analyses in SAP2000<sup>52</sup> conducted on the 3D structure, in absence of the specific base column (Figure 9a). Specifically, the elastic axial contribution of the one-way RC slabs having thickness of 4 cm<sup>35</sup> with the one-way joists of 20 cm is modeled. The orthogonal frames (in the y-z plane) are assumed to have the

same geometrical and mechanical characteristics of the frame under study (in x-z plane). In addition, the torsional and bending stiffness of all the beams and the bending stiffness of the columns are properly reduced according to Refs.<sup>65–67</sup> to consider the nonlinear behavior in a simplified way; the axial and bending stiffness of beams and the bending stiffness of the columns of the frame under study (in x-z plane) are nullified since their contributions are accounted for in the 2D FE model. To compute the stiffness at each node for each floor, a unitary horizontal force in the out-of-plane direction of the orthogonal frame (i.e., x direction) is applied to that node (Figure 9a). The unitary horizontal force divided by the displacement provides the elastic stiffness of the spring at that node. This procedure has been repeated for each node of all the columns apart from the one subjected to the sudden collapse. Then, a spring on each node of the frame under study is applied, as shown in Figure 9b. The numerical values of the stiffnesses are reported in Table 2. This model is denoted as “CS + springs model.”

Figure 10 presents a comparison between these three models, considering the removal of the column C.

With respect to the *STANDARD model*, the continuity of longitudinal rebars (i.e., *C model*) leads to an increase of the ultimate imposed displacement, equal to 30 cm. In fact, the proposed continuity criterion leads to a better redistribution of stresses along the beam length (Figure 10b) because increases the flexural resistance and ductility of the most stressed cross-sections and, thus, it implicates a delay in the strength drop. Moreover, for the increase of the total amount of reinforcement, the flexural peak slightly increases compared to the previous case, reaching a value of 846 kN. Another improvement is that the transition from positive (downward) to negative (upward) vertical displacement of the nodes (Figure 10c) is more pronounced since the more ductile response. This result is in line with Ref.,<sup>12</sup> where it is underlined that if the reinforcement is continuous over

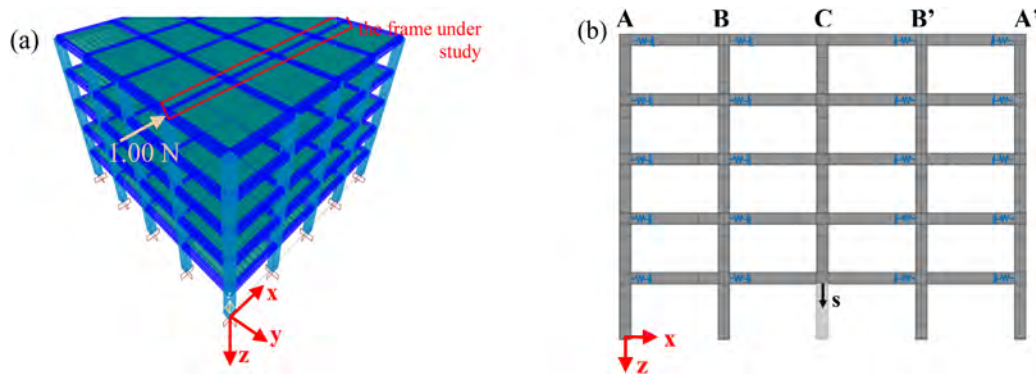


**FIGURE 9** Lateral constraint conditions: (a) 3D structure modeled in SAP 2000: example of calibrating the spring stiffness for the last floor, column A; (b) springs positions (in blue) within the frame under study in ATENA-2D.

**TABLE 2** Elastic spring stiffness for the different floors for column C removal.

	Spring stiffness— column A and A' [N/m]	Spring stiffness— column B and B' [N/m]
1st floor	9.775E+07	9.634E+07
2nd floor	7.143E+07	7.062E+07
3rd floor	5.291E+07	5.247E+07
4th floor	4.122E+07	4.095E+07
5th floor	3.291E+07	3.270E+07

the lateral columns, the structure shows a larger softening. However, no catenary stage occurs: the nodes continue to move outward (horizontal displacement) without any reduction (Figure 10d).

As for the *CS model*, the main outcome is an important recovery in the strength of the post-peak flexural trend with the ultimate resistance that reaches a value of 1153 kN for an ultimate imposed displacement of 77 cm. The flexural peak also increases and equal to 1037 kN. In addition, at a displacement higher than 30 cm there is the beginning of the activation of the catenary behavior for the beams of the frame. The catenary stage activates when the vertical imposed displacement reaches almost the depth of the beam, as observed in the experimental tests.<sup>62</sup> The catenary activation is not only visible from the capacity curve (Figure 10a), but also observing the horizontal and vertical displacements of the beam-column nodes. Regarding the horizontal ones (Figure 10e), the transition from an arching to a catenary behavior implies the shift from compressive to tensile

actions on the beams. This implies that the nodes start to displace inward and downward (Figure 10e,f). Finally, the peak strain reached along the longitudinal reinforcement is equal to the ultimate value of 18% in the upper bars close to the adjacent columns (i.e., columns B and B'). The plot in Figure 10a also shows intermediate values of the reinforcement deformations between 10% and 18%.

Regarding the additional presence of the lateral constraints (i.e., *CS + springs* model), it implies an increase in the flexural peak due to the axial loads acting on the beams, with a flexural peak of 1330 kN. At the same time, the presence of lateral constraints facilitates the transition toward catenary at displacements between 20 and 40 cm. Results in terms of vertical displacements (Figure 10h) of the nodes show that the horizontal springs tend to reduce the arching effects of the beams with respect to the previous cases. In fact, the upward movement proper of the arching phase is less pronounced, while the downward movements that initiate with the catenary stage are more marked. The constraints of nodes are also visible in the horizontal displacements shown in Figure 10g, for which the outward horizontal displacements of the columns A and B are less pronounced with respect to the inward displacements caused by the tying effect of the rebars. The resistance loss registered at a displacement of around 40 cm (Figure 10a) is due to the crushing of concrete in the sections of the beams close to the column B and B'. Finally, the peak strain reached along the longitudinal reinforcement is equal to the ultimate value of 18% in the lower bars of the beams close to column C.

As for the ultimate resistance capacity (i.e.,  $H_{rd}$ ) of the equivalent elastic springs along the horizontal direction corresponding to the ultimate resistance bending moments of the orthogonal beams in the y-z plane, the springs fail for displacements at the end of the catenary path. It should be noted that the resistance capacity

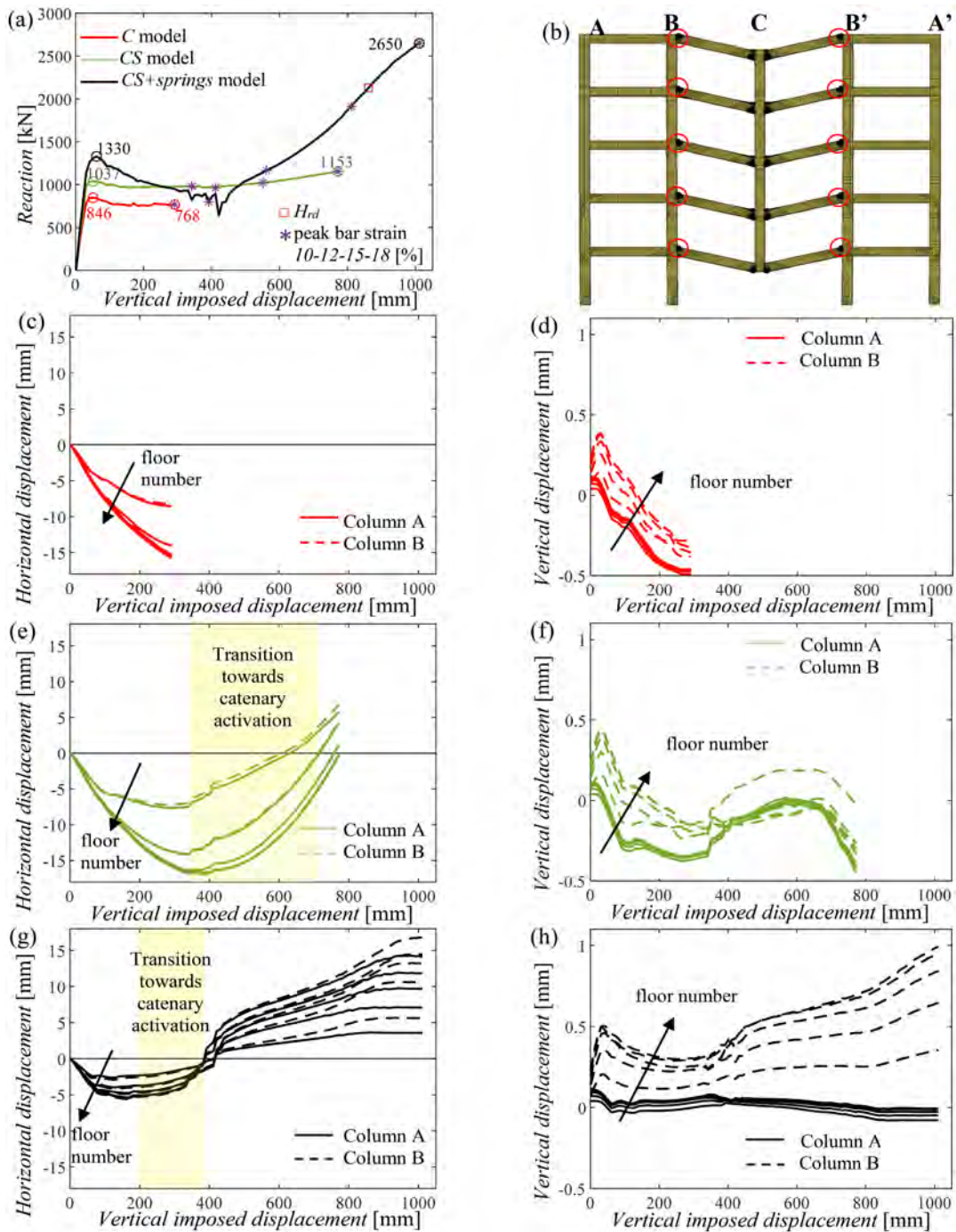


FIGURE 10 Results of the displacement-controlled pushdown analyses: (a) capacity curves; (b) failure mode with the critical regions; (c), (e), (g) horizontal displacements of the beam-column nodes for *C*, *CS*, and *CS + springs* models; (d), (f), (h) vertical displacements of the beam-column nodes for *C*, *CS*, and *CS + springs* models.

associated to the horizontal shear resistance of the orthogonal beams in the  $y$ - $z$  plane is never overcome.

It is noteworthy that by considering the presence of the orthogonal frame (i.e., *CS + springs* model) in addition to continuity and symmetry, the ultimate resistance of the capacity curve as well as the flexural peak increase. Note that the beginning of the activation of the catenary

behavior at a displacement of 20 cm means a rotation angle of 0.04.

On the basis of the energetic approach,<sup>41</sup> the catenary behavior ensures the stability of the performance within a robustness-based design. In fact, since the structural response depends on the equivalence between the external and internal works,<sup>41</sup> it is always desirable that it is

reached for low values of the rotation angle to reduce damage to concrete as required to respect the “life safety” limit state. To this aim, if the catenary effects start earlier, it is easier to find the work equivalence for lower rotation angles. Furthermore, in case of large dynamic features characterizing the progressive collapse, the presence of the catenary behavior is also fundamental for large displacements to avoid the collapse according to the “near-collapse” limit state. It follows that the two essential requirements are to increase the flexural peak optimizing the amount of the rebars as well as anticipate the activation of the catenary. Thus, further improvements, suggested in Section 3, are presented in the following to investigate these two objectives.

### 6.3 | Models with global or partial equality and side face rebars

In this subsection, other new proposals in terms of both equal reinforcement arrangements in the floors and presence of the side face rebars are investigated.

At first, the additional improvement is to adopt an equal configuration of the longitudinal reinforcing bars in all the floors, maintaining the previous criteria of both continuity and section symmetry together with the presence of the springs. This model is denoted as “*CSE + springs*.” Particularly, the aim of adopting the same amount of reinforcement in all the floors is to reduce the mechanical efforts in the lower floors and redistribute the stresses among all the floors. Specifically, 5 $\phi$ 18 rebars are arranged continuously and symmetrically along 1.5 m at two edges in all the beams of the five floors. To respect capacity design principles within the proposed cyclic procedure, this implies that: the stirrup step is 7.5 cm for the dissipative areas in the beams of all the floors and the stirrup diameter of all the beam-column nodes is  $\phi$ 10 with the same step of 5 cm. Again, the longitudinal and transverse reinforcement of the columns remained unchanged. Obviously, the change in the stirrup diameter of the beam-column nodes also implies a modification of the constitutive laws for the confined concrete according to Saatcioglu and Razvi.<sup>59</sup> These modifications are summarized in Figure 11a,b.

Another combination consists in applying the criteria of continuity, symmetry, and floor equality only for the first and the last floor, maintaining only the continuity in the three intermediate ones. This new model is identified as “*CPE + springs*” model. This means to adopt, along 1.5 m at two edges of the beams, (5 + 5) $\phi$ 18 in the first and last floors, (3 + 5) $\phi$ 18 in the second and third floors and (3 + 4) $\phi$ 18 in the fourth floor (Figure 12b). To respect the cyclic design methodology, the following

modifications with respect to the *STANDARD* model have been needed: the stirrup step of the first and last floors, in the dissipative area of the beams, is 7.5 cm and the stirrups diameters for beam-column nodes of columns B, C and B' are 10 mm only for the last floors. The summary of the modifications in terms of constitutive laws, according to Saatcioglu and Razvi,<sup>59</sup> together with the reinforcement arrangements are depicted in Figure 12.

Another improvement regards the adoption of additional rebars to enhance the tying effect of the longitudinal reinforcement, which is beneficial in case of a column loss. With this aim, the side face rebars are added to the *CSE + springs* model, as also suggested in a good design practice. Hence, two levels (placed at around 1/3 and 2/3 of the beam height) of 2 $\phi$ 16 are arranged continuously along each beam length for all the five floors, while maintaining the continuity, section symmetry, and global floor equality. This new model is identified as “*CSE + springs + rebars*” model. This additional reinforcement has been verified for ULSS, SLSs and seismic capacity design verifications, thus no other modifications are applied with respect to the *CSE + springs* model. The section reinforcement characteristics are presented in Figure 11c.

In Figure 13, the results of these three improvements in terms of capacity curves are shown. The transition toward catenary effects is visible from both horizontal (Figure 13b,d,f) and vertical (Figure 13c,e,g) displacements of the beam-column nodes.

It is interesting to observe that by applying the criterion of global floor equality (i.e., *CSE + springs* model), the capacity curve presents a high flexural peak followed by an important catenary phase but the resistance drop persists during the transition from arching to catenary behavior. On the other hand, by adopting the criterion of partial equal reinforcement (i.e., *CPE + springs* model) the resistance drop is considerably reduced but failures of the stirrups close to the central columns occur, at an imposed displacement of around 40 cm. In the *CSE + springs* model, there is an increase of both flexural and ultimate resistance, differently from the *CPE + springs* model, with respect to the *CS + springs* model. In the *CSE + springs* model, the beginning of the transition toward catenary is slightly anticipated (at around 15 cm), as well as in the *CPE + springs* model with the advantage of a reduced amount of reinforcement. Note that any structural response in the transition phase (i.e., around 40 cm) can be unstable due to the resistance drop, especially, for the *CSE + springs* model.

Regarding the adoption of the side face rebars (i.e., *CSE + springs + rebars* model), this drop is completely prevented, since the additional reinforcement

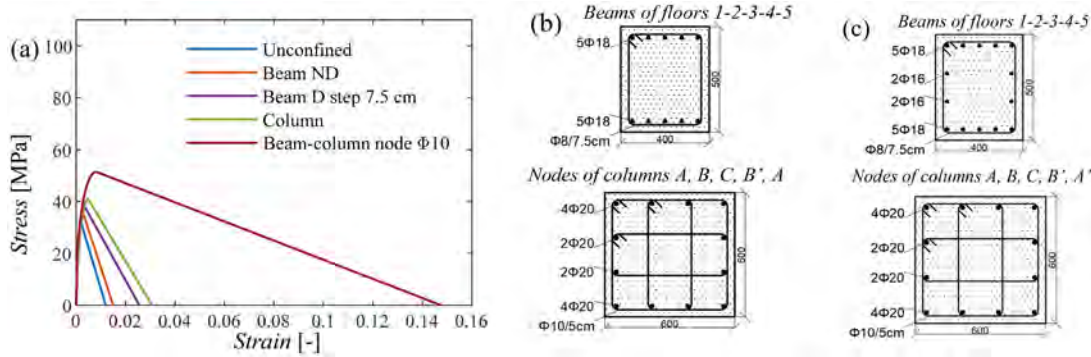


FIGURE 11 (a) Constitutive laws of concrete in compression for both *CSE + springs* model and *CSE + springs + rebars* model; (b) longitudinal and transverse reinforcement in the cross-sections of Figure 3a and in the beam-column nodes for *CSE + springs* model; (c) longitudinal and transverse reinforcement in the cross-sections of Figure 3a and in the beam-column nodes for *CSE + springs + rebars* model.

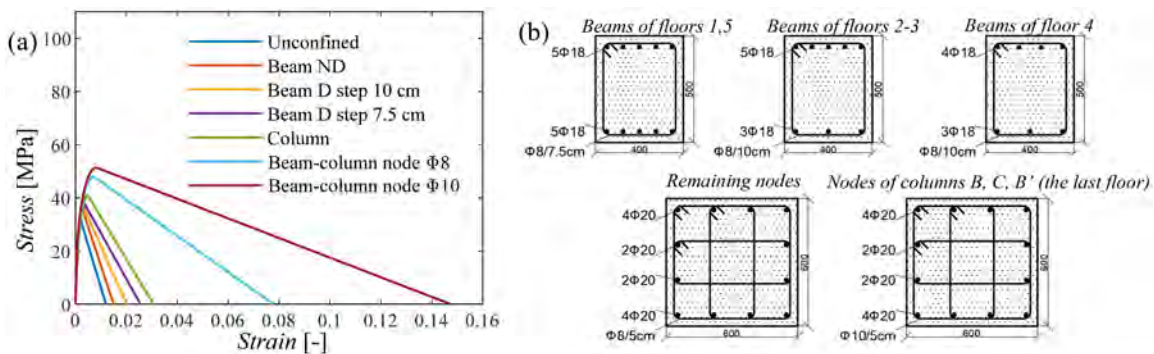


FIGURE 12 *CPE + springs* model: (a) Constitutive laws of concrete in compression; (b) longitudinal and transverse reinforcement of the dissipative area of the beams in the cross-sections of Figure 3a and in the beam-column nodes.

helps in reducing the mechanical effort at the concrete level. This means a reduced damage level of the RC frame. In addition, both flexural peak and ultimate resistance increase. Another very important advantage provided by the side face rebars is that the beginning of the transition toward catenary effect starts considerably earlier than the previous cases, that is, at a displacement of around 10 cm (i.e., meaning a rotation angle of around 0.02). In fact, Figure 13b,d,f demonstrate that the catenary effect is activated more than 10 cm earlier when the side face rebars are included.

The ultimate strain for the longitudinal reinforcement (i.e., 18%) is reached in the lower bars close to the central column for the *CSE + springs* model and *CPE + springs* model, while it occurs in the upper side face rebars close to the columns B and B' for the *CSE + springs + rebars* model. Figure 13a shows also intermediate values of the reinforcement deformations between 10% and 18%.

The ultimate bending resistance of the orthogonal beams is reached at the end of the catenary path for both *CSE + springs* and *CPE + springs* models, while is never

reached in *CSE + springs + rebars* model. In this way, it is underlined that if the side face rebars are added in the orthogonal frames, there is also the advantage that the ultimate bending resistance is never overcome in the orthogonal beams. The resistance capacity associated to the horizontal shear resistance is never overcome.

## 6.4 | Combinations of the improvements for minimum design suggestions

The previous subsections have demonstrated how the longitudinal reinforcement arrangement plays an important role in developing the catenary effect and guarantying enough resistance against the accidental column loss. However, the increase of the total amount of reinforcement with respect to the *STANDARD* design can be seen conflictual with sustainability principles, especially, regarding the economic issue. For this reason, different design strategies with different combinations of the proposed improvements are also considered in this subsection.

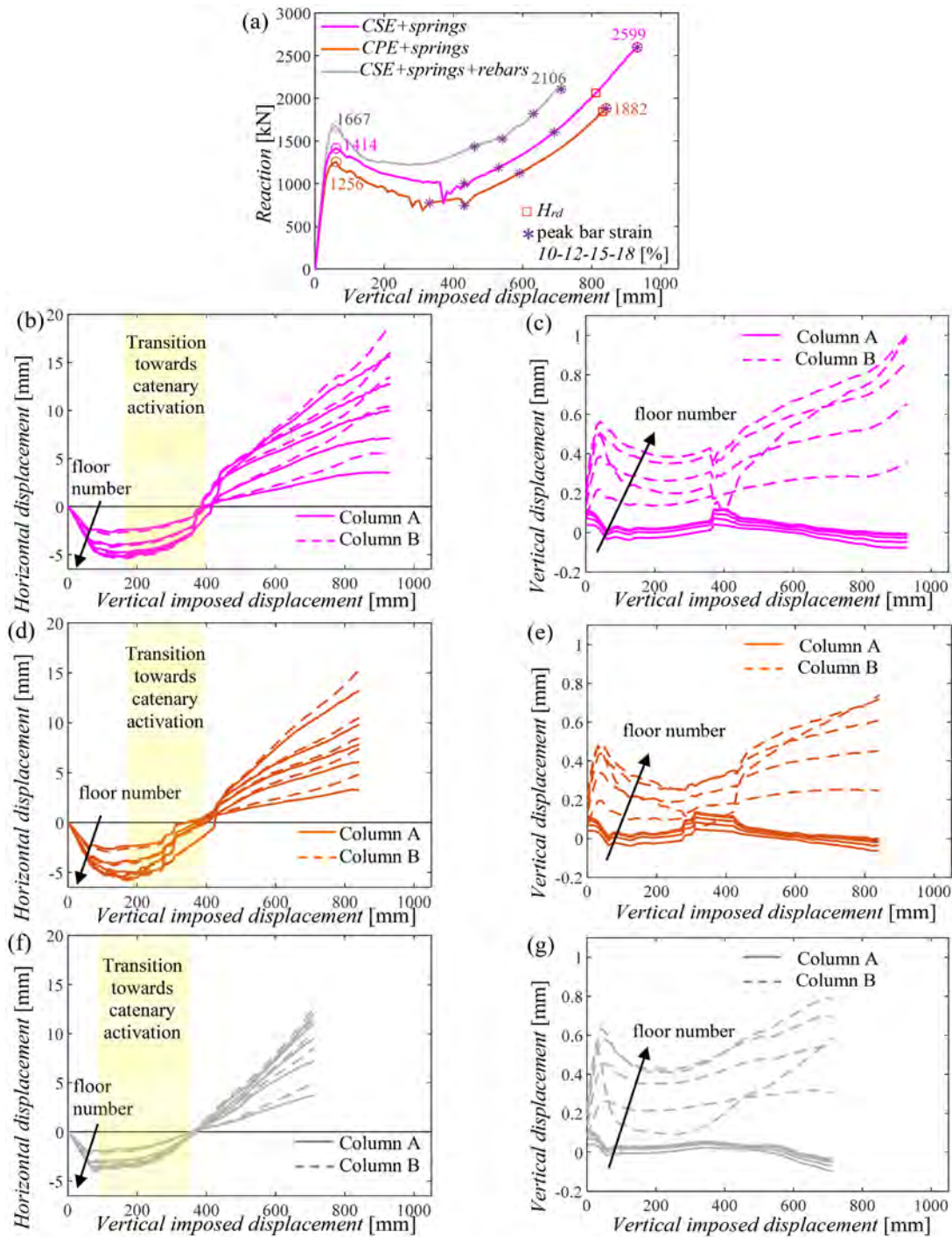


FIGURE 13 Results of the pushdown analyses for the column C removal: (a) capacity curves; (b), (d), (f) horizontal displacements of the beam-column nodes for *CSE + springs*, *CPE + springs* and *CSE + springs + rebars* models; (c), (e), (g) vertical displacements of the beam-column nodes for *CSE + springs*, *CPE + springs*, and *CSE + springs + rebars* models.

One proposal is to consider the continuity together with the presence of two levels (placed at around 1/3 and 2/3 of the beam height) of  $2\phi 16$  as side face rebars in all the five floors in addition to the lateral springs (Figure 14b). This new model is identified as “*C + springs + rebars*.” The additional presence of the side face rebars implies a change in the stirrup step of the dissipative area for the beams in

all the floors from 10 to 7.5 cm, to respect the seismic verifications within the cyclic design approach. The other structural elements were verified and are the same of the *C model*. These modifications, according to Saatcioglu and Razvi,<sup>59</sup> are shown in Figure 14.

The other proposal is to add the side face rebars in all the five floors to the model with partial floor equality,



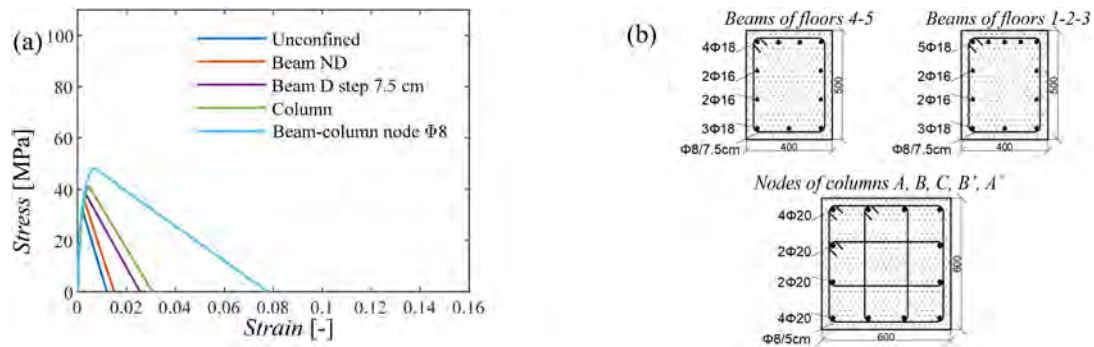


FIGURE 14  $C + springs + rebars$  model: (a) Constitutive laws of concrete in compression; (b) longitudinal and transverse reinforcement of the dissipative area of the beams in the cross-sections of Figure 3a and in the beam-column nodes.

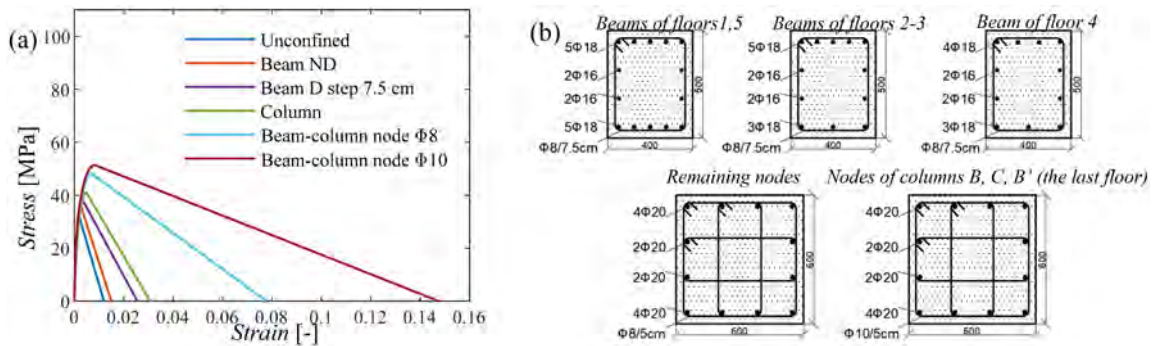


FIGURE 15  $CPE + springs + rebars$  model: (a) Constitutive laws of concrete in compression; (b) longitudinal and transverse reinforcement of the dissipative area of the beams in the cross-sections of Figure 3a and in the beam-column nodes.

herein defined as  $CPE + springs + rebars$  model (Figure 15b). In this case, to respect the capacity design principles, it was necessary to change the stirrups step from 10 to 7.5 cm in the remaining floors with respect to the  $CPE + springs$  model (Section 6.3). The modifications, according to Saatcioglu and Razvi,<sup>59</sup> are shown in Figure 15.

The results of these new two models for the first failure scenario (i.e., the removal of column C), are shown in Figure 16. In both cases, the flexural peaks and ultimate resistances are higher than the corresponding values of the  $CS + springs$  model, whereas the flexural peaks are lower with respect to the  $CSE + springs + rebars$  model. In both models, the activation of catenary response permits to reach a stable structural performance. In detail, the transition to catenary behavior activates at a displacement of around 15 cm with a rotation angle of around 0.03 in both models. These last two results are very important and are similar to the displacement achieved in the  $CSE + springs + rebars$  model. Failures of the stirrups close to the collapsed column are registered during the post-transition phase at an imposed displacement of around 45 cm for the  $CPE + springs + rebars$  model, after the catenary activation. Figure 16a

also shows the different levels of deformation in the rebars for increasing vertical displacement.

It is noteworthy that the presence of side face rebars is also beneficial in reducing the resistance gap between the flexural peak and the resistance of the capacity curve during the transition toward catenary action. This is essential to find a stable energy equivalence<sup>41</sup> since the lower the gap, the larger is the internal energy provided by the structure in case of sudden column loss.

All these aspects emphasize the important role of the side face rebars in anticipating the catenary effects, because their presence permits to reach a stable response earlier with the possibility to reduce the damage level in concrete regarding both “life-safety” and “near-collapse” LSs. Additionally, the combination of the continuity together with partial floor equality represents an effective alternative strategy in substitution of the symmetry suggestion to limit the increase of the longitudinal rebars.

The ultimate bending resistance of the orthogonal beams is reached at the end of the catenary path for both models, while is never overcome in the orthogonal beams if side face rebars are considered in the orthogonal frames. At the same time, the resistance capacity associated to the horizontal shear resistance is never overcome.

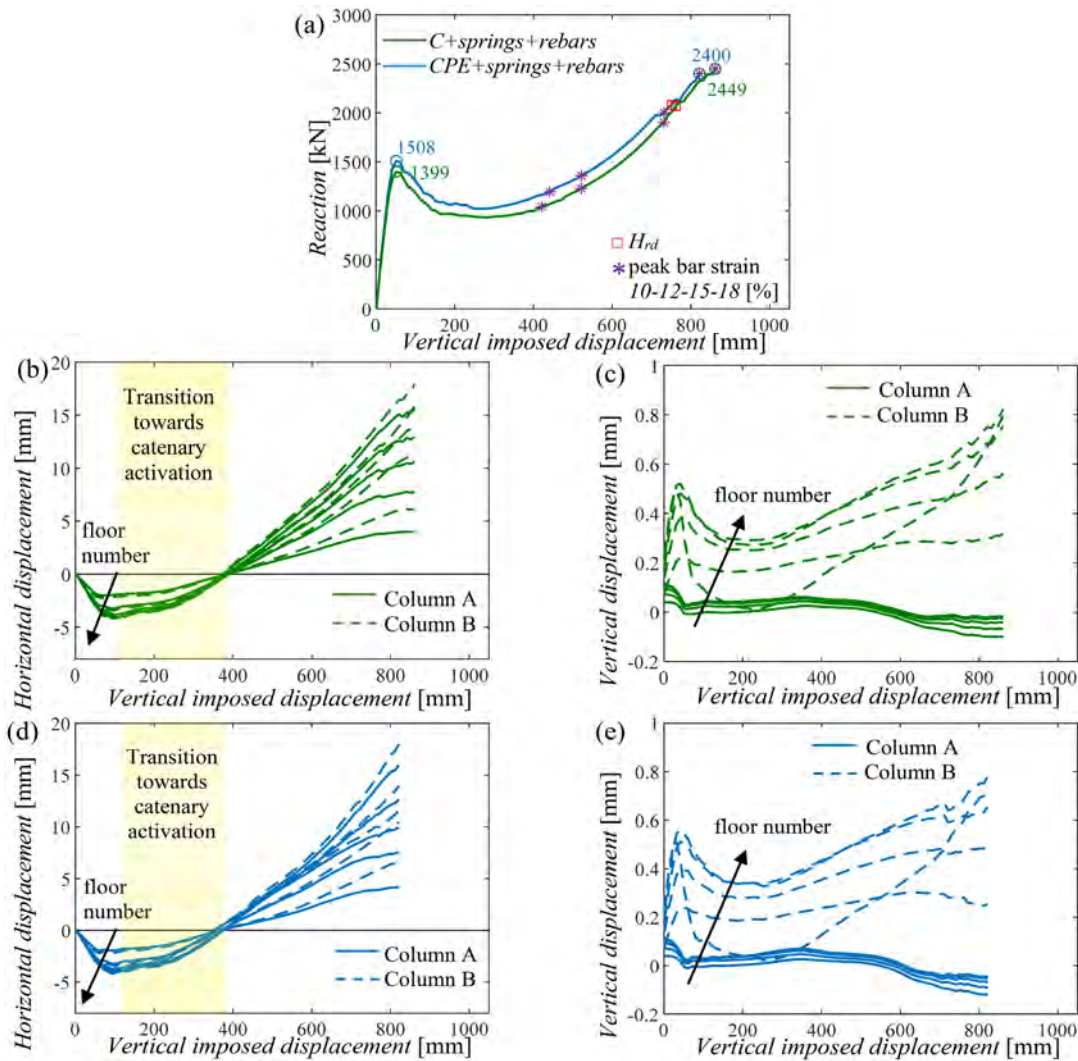


FIGURE 16 Results of the displacement-controlled pushdown analyses for the column C removal: (a) capacity curves; (b) and (d) horizontal displacements of the beam-column nodes for  $C + springs + rebars$  and  $CPE + springs + rebars$  models; (c) and (e) vertical displacements of the beam-column nodes for  $C + springs + rebars$  and  $CPE + springs + rebars$  models.

## 7 | THE SECOND FAILURE SCENARIO: NLFE ANALYSES OF THE RC MR FRAME FOR SOME ROBUSTNESS IMPROVEMENTS

This section describes the second failure scenario with the removal of column B. In detail, some useful robustness suggestions proposed for the first failure configuration are herein tested for the second failure scenario. According to the procedure explained in Section 6.2, the springs have been re-calibrated as shown in Figure 17 and the corresponding values are listed in Table 3.

The results in terms of capacity curves for the second failure scenario (i.e., removal of column B) are shown in Figures 18 and 19 considering the same combinations of the proposed improvements discussed, respectively, in

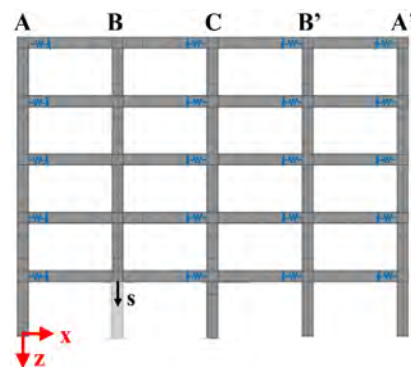


FIGURE 17 Springs positions (in blue) within the frame under study in ATENA-2D for the second failure scenario.

Section 6.2 (i.e.,  $CSE + springs$ ,  $CPE + springs$ , and  $CSE + springs + rebars$  models) and Section 6.3 (i.e.,  $C + springs + rebars$  and  $CPE + springs + rebars$  models).

**TABLE 3** Elastic spring stiffness for the different floors for column B removal.

	Spring stiffness column A [N/m]	Spring stiffness column C [N/m]	Spring stiffness column B' [N/m]	Spring stiffness column A' [N/m]
1st floor	7.468E+06	9.747E+07	1.685E+08	9.766E+07
2nd floor	7.210E+06	7.128E+07	1.031E+08	7.138E+07
3rd floor	6.954E+06	5.283E+07	6.854E+07	5.288E+07
4th floor	6.684E+06	4.119E+07	5.013E+07	4.120E+07
5th floor	6.309E+06	3.288E+07	3.837E+07	3.289E+07

Since this column removal implies a lower contribution provided by the orthogonal frames, the flexural peaks are relatively lower with respect to the same models of the first failure scenario as well as the catenary effect is less pronounced with a delay in the beginning. As observed in Figure 18a, the same deformation levels in the reinforcement rebars are achieved for lower displacements in comparison with the first failure scenario.

Similar conclusions can be drawn regarding the side face rebars: their presence is able to increase the flexural peak and anticipates the beginning of the transition toward the catenary effects (i.e., at a displacement of around 20 cm—Figure 18f), if compared to the cases where the side face rebars are absent (i.e., at displacements of around 35 cm—Figure 18b,d). In addition, failure of the stirrups occurs at 45 and 40 cm for the *CSE + springs + rebars* and *CPE + springs + rebars* models, respectively.

As for the minimum design suggestions (Figure 19), the flexural peaks are slightly lower with respect to the *CSE + springs + rebars* model and the transition to catenary occurs for displacements slightly higher than 20 cm for the *C + springs + rebars* and *CPE + springs + rebars* models. Even in these models, a failure of the stirrups in the beams close to the collapsed column is registered at a displacement of around 35 cm for the *C + springs + rebars* model and around 45 cm for the *CPE + springs + rebars* model.

In the second failure scenario, the ultimate bending resistance of the orthogonal frame is reached for lower displacements with respect to the first failure scenario. However, the side face rebars in the orthogonal beams permit to postpone the failures at larger displacements. The resistance capacity associated to the horizontal shear resistance is never overcome.

It can be deduced that the continuity and partial floor equality, in substitution of the symmetry, combined with the side face rebars can represent a good compromise between robustness and sustainability principles also for

the second failure scenario, since it is possible to reach a high flexural resistance followed by a catenary behavior adopting a lower amount of reinforcement with respect to other solutions.

It is noteworthy to highlight that reliability analyses combined with an energetic approach<sup>41</sup> are necessary to validate the conclusions derived from the both failure scenarios by determining the safety level for the different design suggestions herein proposed.

## 8 | CONCLUSIONS

The study has concerned a parametric analysis on 2D RC MR frames, designed in a highly seismic area. Numerical results have shown that the seismic criteria and construction details adopted following the current code rules, although they may be favorable with regard to robustness, cannot be sufficient to avoid a disproportionate collapse in case of loss of a base column.

Subsequently, some design improvements are suggested respecting always the seismic design code provisions by means of a cyclic design procedure. In detail, considering the influence of the lateral stiffness of the orthogonal frames, different configurations of the longitudinal reinforcement bars of the beam have been proposed in order to take advantages of the continuity and Vierendeel effects in the floors as well as the benefits of accounting for the side face reinforcement bars in the beams. For the different combinations of the proposed suggestions, 2D NLFE pushdown analyses of the whole frames have been performed by imposing a monotonically increasing vertical displacement at the point of the column removal. Two failure scenarios have been examined. Specifically, numerical simulations on the frames characterized by the proposed design modifications regarding the longitudinal reinforcement of the beams (i.e., continuity, global or partial equality in the floors in addition or in substitution of the symmetry) have revealed a great improvement for the robust behavior in

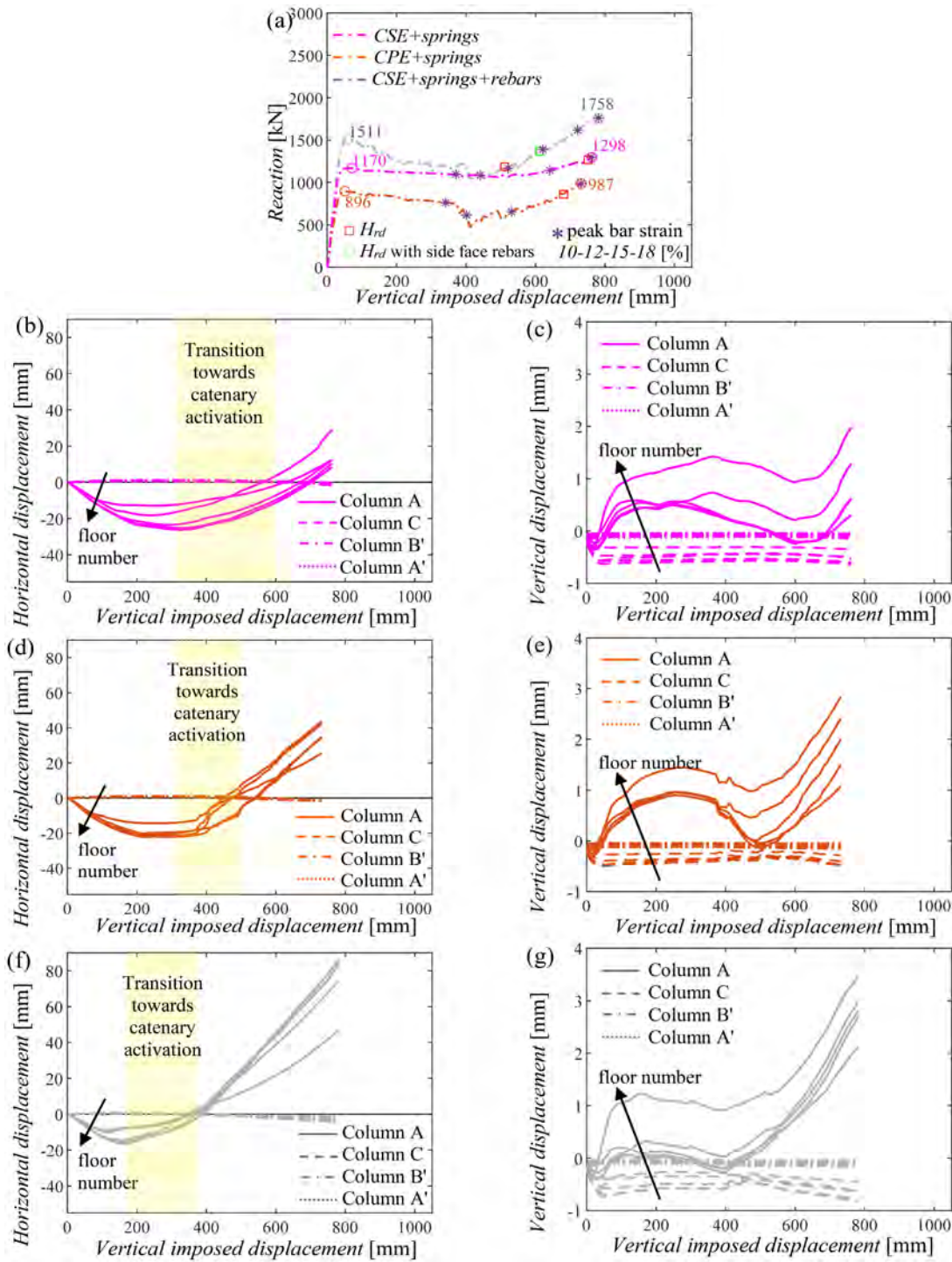


FIGURE 18 Results of the pushdown analyses for the column B removal: (a) capacity curves; (b), (d), (f) horizontal displacements of the beam-column nodes for *CSE + springs*, *CPE + springs*, and *CSE + springs + rebars* models; (c), (e), (g) vertical displacements of the beam-column nodes for *CSE + springs*, *CPE + springs*, and *CSE + springs + rebars* models.

terms of both flexural and catenary response. Furthermore, the numerical outcomes have demonstrated the very useful role of the side face rebars in increasing the flexural peak and anticipating the transition to

catenary behavior for displacements equal to 10 or 20 cm (i.e., rotation angle of 0.02 or 0.04), as function of the considered failure scenario. By this way, a reduction of the damage level in the RC frame can be achieved with a

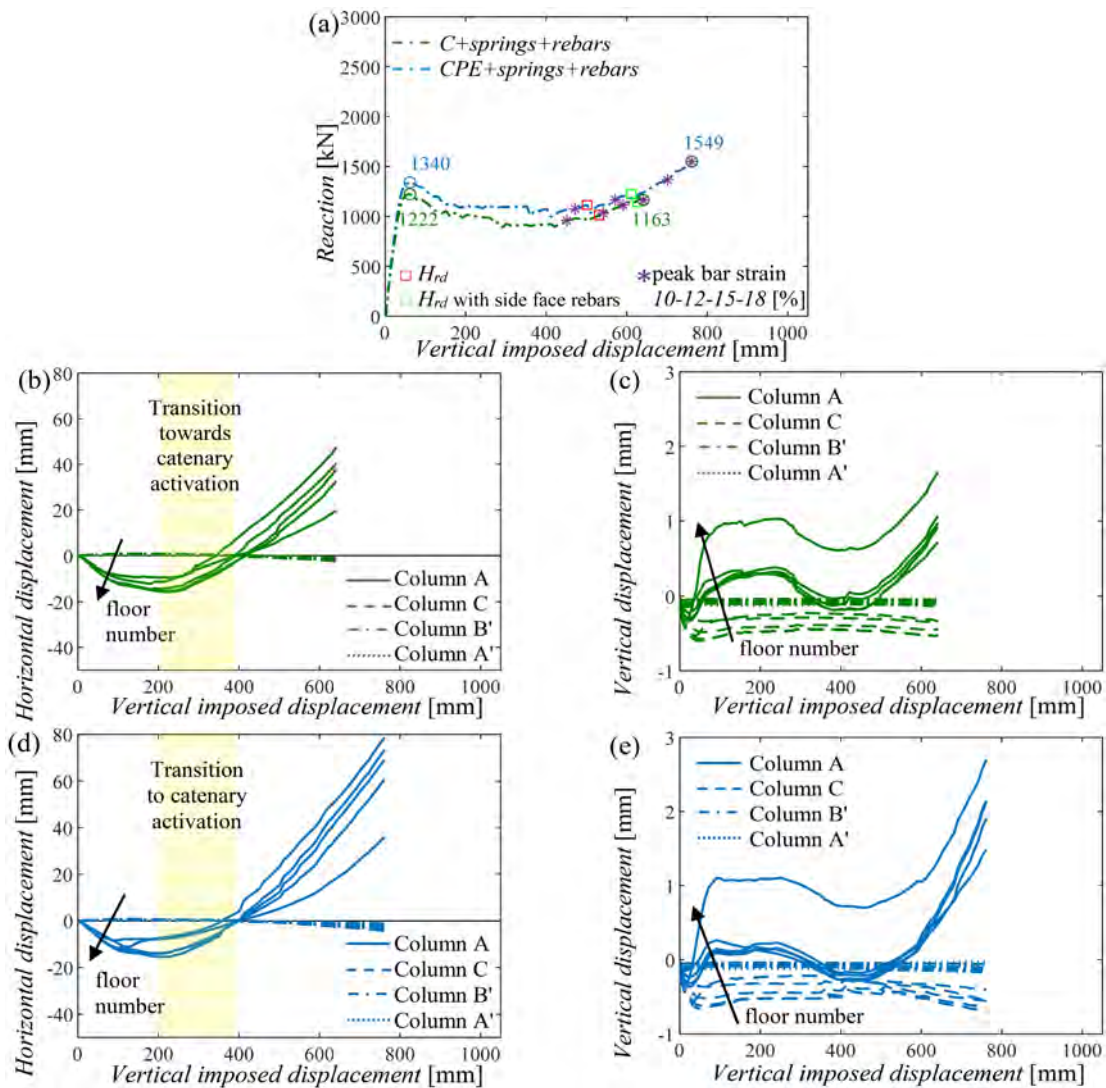


FIGURE 19 Results of the pushdown analyses for the column B removal: (a) capacity curves; (b) and (d) horizontal displacements of the beam-column nodes for  $C + \text{springs} + \text{rebars}$  and  $CPE + \text{springs} + \text{rebars}$  models; (c) and (e) vertical displacements of the beam-column nodes for  $C + \text{springs} + \text{rebars}$  and  $CPE + \text{springs} + \text{rebars}$  models.

stable structural response even in the case of large displacements. Another important role of the side face rebars is to guarantee the ultimate resistance of the beams in the orthogonal frames, as demonstrated, especially, for the second failure scenario. It follows that these achievements can be very functional to respect both life safety and near-collapse LSs.

Other considerations have followed in order to reduce the total amount of reinforcement by providing minimum design suggestions able to ensure an adequate robustness in line with sustainability principles. These different design strategies have also demonstrated to be very effective in terms of both flexural peak and catenary behavior. Specifically, the continuity and partial floor equality, in substitution of the symmetry, combined with the side face rebars can represent a good compromise

between robust and sustainability principles, as demonstrated for the both failure scenarios. These solutions permit to reach a high flexural resistance, followed by a catenary behavior for rotation angles between 0.03 and 0.04, as function of the considered failure scenario, adopting a lower amount of reinforcement with respect to other solutions.

All the abovementioned advantages deriving from the proposed design suggestions are effective to increase the robustness by improving the mechanical response of a frame within a 3D building. This is very useful in any structure and can be functional, especially, for buildings where slabs present joists along only one direction. Moreover, the outcomes showed the compatibility between robustness and earthquake engineering criteria through the proposed cyclic design

procedure. With the scope to select the most appropriate combination between the different design suggestions, reliability analyses combined with an energetic approach are necessary to determine the corresponding safety level.

## ACKNOWLEDGMENTS

This study was carried out within the RETURN Extended Partnership and received funding from the European Union Next-GenerationEU (National Recovery and Resilience Plan—NRRP, Mission 4, Component 2, Investment 1.3—D.D. 1243 2/8/2022, PE0000005).

This work is also part of the collaborative activity developed by the authors within the research project “RELUIS—Contributi normativi relativi a Costruzioni Esistenti in Cemento Armato—WP11.4.”

## DATA AVAILABILITY STATEMENT

The data that support the findings of this study are available from the corresponding author upon reasonable request.

## ORCID

Elena Miceli  <https://orcid.org/0000-0002-1262-3403>

Paolo Castaldo  <https://orcid.org/0000-0002-7956-9392>

## REFERENCES

- Adam JM, Parisi F, Sagaseta J, Lu X. Research and practice on progressive collapse and robustness of building structures in the 21st century. *Eng Struct.* 2018;173:122–49.
- Starossek U. Progressive collapse of structures: nomenclature and procedures. *Struct Eng Int.* 2016;16(2):113–7.
- Castaldo P, Mancini G, Palazzo B. Seismic reliability-based robustness assessment of three-dimensional reinforced concrete systems equipped with single-concave sliding devices. *Eng Struct.* 2018;163:373–87.
- European Committee for Standardization. Eurocode – basis of structural and geotechnical design. 1990.
- General Services Administration (GSA). Progressive collapse analysis and design guidelines. Washington, DC: Office of Chief Architects; 2003.
- Department of Communities and Local Government. The building regulations 2010 – structure: approved document a. UK: HM Government; 2010.
- ASCE Standard 7-02. Minimum design loads for buildings and other structures (ASCE 7–16). Reston, VA: American Society of Civil Engineers; 2016.
- General Services Administration (GSA). Alternative path analysis and design guidelines for progressive collapse resistance. Washington, DC: Office of Chief Architects; 2013.
- Australian Building Codes Board (ABCB). National construction code (NCC). Canberra, Australia: Council of Australian Governments; 2016.
- China Association for Engineering Construction Standardization (CECS). Code for anti-collapse design of building structures. Vol 392. Beijing, China: CECS; 2014.
- United States Department of Defence (DoD), Unified Facilities Criteria (UFC): design of buildings to resist progressive collapse, Washington, D.C. 2016.
- Consiglio Nazionale delle Ricerche, Istruzioni per la valutazione della robustezza delle costruzioni. 2018.
- Parisi F, Augenti N. Influence of seismic design criteria on blast resistance of RC framed buildings: a case study. *Eng Struct.* 2012;44:78–93.
- Brunesi E, Nascimbene R, Parisi F, Augenti N. Progressive collapse fragility of reinforced concrete framed structures through incremental dynamic analysis. *Eng Struct.* 2015;104:65–79.
- Ren P, Li Y, Lu X, Guan H, Zhou Y. Experimental investigation of progressive collapse resistance of one-way reinforced concrete beam–slab substructures under a middle-column-removal scenario. *Eng Struct.* 2016;118:28–40.
- Lu X, Lin K, Li Y, Guan H, Ren P, Zhou Y. Experimental investigation of RC beam-slab substructures against progressive collapse subject to an edge-column-removal scenario. *Eng Struct.* 2017;149:91–103.
- Adam JM, Buitrago M, Bertolesi E, Sagaseta J, Moragues JJ. Dynamic performance of a real-scale reinforced concrete building test under a corner-column failure scenario. *Eng Struct.* 2020;210:110414.
- Zhang L, Zhao H, Wang T, Chen Q. Parametric analysis on collapse-resistance performance of reinforced-concrete frame with specially shaped columns under loss of a corner column. *Open Constr Build Technol J.* 2016;10(1):466–80.
- Belletti B, Damoni C, Cervenka V, Hendriks MAN. Catenary action effects on the structural robustness assessment of RC slab strips subjected to shear and tensile forces. *Mag Concr Res.* 2019;71(20):1083–96.
- Tan Z, Zhong W-h, Meng B, Zheng Y-h, Duan S-c. Effect of various boundary constraints on the collapse behavior of multi-story composite frames. *J Build Eng.* 2022;52:104412. <https://doi.org/10.1016/j.jobte.2022.104412>
- Wang Y, Zhang B, Xiang-Lin G, Lin F. Experimental and numerical investigation on progressive collapse resistance of RC frame structures considering transverse beam and slab effects. *J Build Eng.* 2022;47:103908.
- Fascetti A, Kunnath SK, Nisticò N. Robustness evaluation of RC frame buildings to progressive collapse. *Eng Struct.* 2015;86:242–9.
- Brunesi E, Parisi F. Progressive collapse fragility models of European reinforced concrete framed buildings based on push-down analysis. *Eng Struct.* 2017;152:579–96.
- Di Trapani F, Giordano L, Mancini G. Progressive collapse response of reinforced concrete frame structures with masonry infills. *J Eng Mech.* 2020;146(3):04020002-1–04020002-19.
- Asprone D, de Risi R, Manfredi G. Defining structural robustness under seismic and simultaneous actions: an application to precast RC buildings. *Bull Earthq Eng.* 2016;14(2):485–99.
- Izzuddin BA, Sio J. Rational horizontal tying force method for practical robustness design of building structures. *Eng Struct.* 2022;252:113676.
- Colombo M, Martinelli P, di Prisco M. A design approach to evaluate the load-carrying capacity of reinforced concrete slabs considering tensile membrane action. *Struct Eng Int.* 2021;31(2):260–70.

28. Martinelli P, Colombo M, Ravasini S, Belletti B. Application of an analytical method for the design for robustness of RC flat slab buildings. *Eng Struct*. 2022;258:114117.
29. Pham AT, Tan KH. A simplified model of catenary action in reinforced concrete frames under axially restrained conditions. *Mag Concr Res*. 2017;69:1115–34.
30. Gurley C. Progressive collapse and earthquake resistance. *Pract Period Struct Design Constr*. 2008;13(1):19–23.
31. Hayes JR, John R, Woodson SC, Pekelnicky RG, Poland CD, Corley WG, et al. Can strengthening for earthquake improve blast and progressive collapse resistance? *J Struct Eng*. 2005; 131(8):1157–77.
32. Tsai M, Lin B. Investigation of progressive collapse resistance and inelastic response for an earthquake-resistant RC building subjected to column failure. *Eng Struct*. 2008;30:3619–28.
33. Corley WG. Applicability of seismic design in mitigating progressive collapse. In: proceedings of workshop on prevention of progressive collapse. Washington (DC): National Institute of Building Sciences; 2002.
34. Corley WG Sr, Mlakar PF, Sozen MA, Thornton CH. Oklahoma City bombing: summary and recommendations for multihazard mitigation. *J Perform Constr Facil*. 1998;12(3):100–12.
35. MIT, Istruzioni per l'applicazione dell' Aggiornamento delle "Norme tecniche per le costruzioni" di cui al decreto ministeriale 17 gennaio 2018. 2019.
36. European Committee for Standardization. Eurocode 8 – Design of Structures for earthquake resistance. 1998.
37. Tsai MH, Lin BH. Dynamic amplification factor for progressive collapse resistance analysis of an RC building. *Struct Design Tall Spec Build*. 2009;18(5):539–57.
38. Marjanishvili SM. Progressive analysis procedure for progressive collapse. *J Perform Constr Facil*. 2004;18(2):79–85.
39. Khandelwal KS, El-Tawil S. Pushdown resistance as a measure of robustness in progressive collapse analysis. *Eng Struct*. 2011; 33(9):2653–61.
40. Ferraioli M, Avossa AM, Mandara A. Assessment of progressive collapse capacity of earthquake-resistant steel moment frames using pushdown analysis. *Open Constr Build Technol J*. 2014;8(1):324–36.
41. Izzuddin BA, Vlassis AG, Elghazouli AY, Nethercot DA. Progressive collapse of multi-storey buildings due to sudden column loss – part I: simplified assessment framework. *Eng Struct*. 2008;30(5):1308–18.
42. Lew HS, Bao Y, Sadek F, Main JA, Pujol S, Sozen MA. An experimental and computational study of reinforced concrete assemblies under a column removal scenario. Vol 1720. Washington, DC: NIST Technical Note; 2011. p. 106.
43. Lim NS, Tan KH, Lee CK. Effects of rotational capacity and horizontal restraint on development of catenary action in 2-D RC frames. *Eng Struct*. 2017;153:613–27.
44. Yu J, Tan KH. Structural behavior of RC beam-column subassemblages under a middle column removal scenario. *J Struct Eng*. 2013;139(2):233–50.
45. Yu J, Tan KH. Experimental and numerical investigation on progressive collapse resistance of reinforced concrete beam column sub-assemblages. *Eng Struct*. 2013;55:90–106.
46. Kaewkulchai G, Williamson EB. Beam element formulation and solution procedure for dynamic progressive collapse analysis. *Comput Struct*. 2004;82(7–8):639–51.
47. Xuan DP, Tan KH. Experimental study of beam-slab substructures subjected to a penultimate-internal column loss. *Eng Struct*. 2013;55:2–15.
48. Belletti B, Muttoni A, Ravasini S, Vecchi F. Parametric analysis on punching shear resistance of reinforced concrete continuous slabs. *Mag Concr Res*. 2018;71(20):1083–96.
49. Botte W, Gouverneur D, Caspeepele R, Taerwe L. Influence of design parameters on tensile membrane action in reinforced concrete slabs. *Struct Eng Int*. 2015;2015(1):50–60.
50. Braestrup MW. Dome effect in RC slabs: rigid-plastic. *ASCE J Struct Div*. 1989;106(ST6):1237–53.
51. Cantone R, Belletti B, Manelli L, Muttoni A. Compressive membrane action effects on punching strength of flat RC slabs. *Key Eng Mater*. 2016;711:698–705.
52. CSI. SAP2000 Integrated software for structural analysis and design. Berkeley, CA: Computers and Structures Inc.; 2016.
53. Cervenka Consulting s.r.o. ATENA 2D v5, Prague, Czech Republic. 2014.
54. Hendriks MAN, Roosen MA, editors. Guidelines for nonlinear finite element analysis of concrete structures. Utrecht, Netherlands: Rijkswaterstaat Centre for Infrastructure. Report RTD: 1016-1:2019; 2019.
55. Gino D, Castaldo P, Giordano L, Mancini G. Model uncertainty in non-linear numerical analyses of slender reinforced concrete members. *Struct Concr*. 2021;22(2):845–70.
56. Cervenka V. Constitutive model for cracked reinforced concrete. *J ACI*. 1985;82(6):877–82.
57. Darwin D, Pecknold DAW. Inelastic model for cyclic biaxial loading of reinforced concrete. Civil Engineering Studies, University of Illinois, July. 1974 Available from <https://www.ideals.illinois.edu/bitstream/handle/2142/13822/SRS-409.pdf?sequence=2>
58. CEB-FIP Model Code 1990, First Draft, Committee Euro-International du Beton, Bulletin d'information No. 195,196, Mars.
59. Saatcioglu M, Razvi SR. Strength and ductility of confined concrete. *J Struct Eng*. 1993;119(10):3109–10.
60. Dyngeland T. Behavior of reinforced concrete panels, dissertation, Trondheim university, Norway. BK-Report. 1989;1989:1.
61. Kolmar W. Beschreibung der Kraftuebertragung über Risse in nichtlinearen Finite-Element-Berechnungen von Stahlbetontragwerken. 1986 Dissertation, T.H. Darmstadt, p. 94.
62. Massicotte B, Elwi AE, MacGregor JG. Tension-stiffening models for planar reinforced concrete members. *J Struct Eng*. 1990;116(11):3039–58.
63. Qian K, Li B, Ma JX. Load-carrying mechanism to resist progressive collapse of RC buildings. *J Struct Eng*. 2015;141(2): 1–14.
64. Caprili S, Salvatore W. Mechanical performance of steel reinforcing bars in uncorroded and corroded conditions. *Data Brief*. 2018;18:1677–95.
65. Avşar Ö, Bayhan B, Yakut A. Effective flexural rigidities for ordinary reinforced concrete columns and beams. *Struct Des Tall Spec Build*. 2014;23(6):463–82.
66. Castaldo P, De Iuliis M. Effects of deep excavation on seismic vulnerability of existing reinforced concrete framed structures. *Soil Dyn Earthq Eng*. 2014;64:102–12.
67. American Society of Civil Engineers (ASCE) for the Federal Emergency Management Agency. Pre-standard and commentary for the seismic rehabilitation of buildings, FEMA Report 356. Washington, DC 2000.

## AUTHOR BIOGRAPHIES



**Elena Miceli**, Department of Structural, Geotechnical and Building Engineering (DISEG), Politecnico di Torino, Turin, Italy. Email: [elena.miceli@polito.it](mailto:elena.miceli@polito.it).



**Paolo Castaldo**, Department of Structural, Geotechnical and Building Engineering (DISEG), Politecnico di Torino, Turin, Italy. Email: [paolo.castaldo@polito.it](mailto:paolo.castaldo@polito.it) and [pcastaldo@unisa.it](mailto:pcastaldo@unisa.it).

**How to cite this article:** Miceli E, Castaldo P. Robustness improvements for 2D reinforced concrete moment resisting frames: Parametric study by means of NLFE analyses. *Structural Concrete*. 2024;25(1):9–31. <https://doi.org/10.1002/suco.202300443>